Wave Forces on Slender Submarine Pipelines

Bibliography

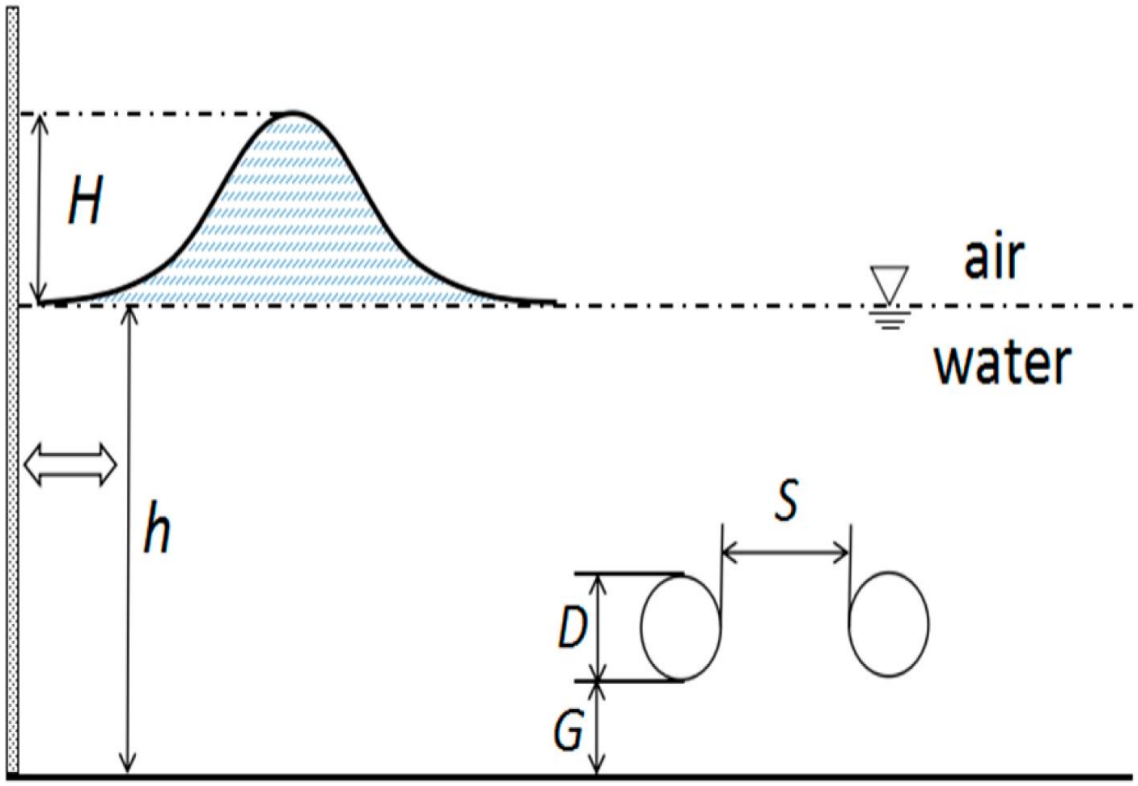

Prepared by
Fawzia Al-Buloushi

KUWAIT INSTITUTE FOR SCIENTIFIC RESEARCH

NATIONAL SCIENTIFIC & TECHNICAL INFORMATION CENTER

TECHNICAL SERVICES DEPARTMENT

August 2022

Table of Content

Introduction

Should the pipeline be incapable of withstanding imposed hydrodynamic loads it will be displaced and may even be ruptured. Such failures are costly, and since pipelines often convey sewage, oil or harmful chemicals, the resulting pollution may be anything between inconvenient and catastrophic. On the other hand, if the pipe is overdesigned and constructed to conservative standards, the excess expenditure may be large and quite unjustified. A popular method of protecting a pipe from wave effects in "shallow" water is to bury it. But at what water depth does one cease this practice? Grace (1971) has reported the displacement of pipelines in depths of as much as 70 m. Burying the pipe in a sandy sea bed is no foolproof protection either - according to Alterman (1962), for instance, 2,5 m changes in sea bed level have been observed at the site of a pipeline in the Mediterranean. For almost three decades, researchers have studied wave forces on rigid bodies, notably cylinders. The problem is by no means solved yet. A submarine pipeline is a special type of cylindrical structure, namely a cylinder near a solid boundary for which the results of general investigations are not necessarily valid. Consequently, even less,. positive information is available regarding wave forces on pipelines. This particular subject has, however, been receiving more and more attention in recent years.

Numerous theories have been developed to describe wave phenotnena; some are better than others in certain respects, but all the theories have shortcomings in some regards. The main reason is the extreme complexity of ocean waves - especially in the coastal zone - which is difficult to describe mathematically. Other reasons include the three dimensional characteristics and apparent random behavior of water waves.

This Bibliography is a search from 2022

Abstracts

1) **Experimental study on dynamic responses of a deep-sea mining system**
Wu, Q., Yang, J., Guo, X., (...), Lu, W., Lu, H., 2022 Ocean Engineering 248,110675

Abstract
The global demand for minerals has raised interest in the design and study of Deep-Sea Mining (DSM) systems for minerals. In this study, the global dynamic responses of a DSM system are investigated using a scaled model test in an ocean basin. Vessel movements, loads of rigid pipe, and buffer accelerations were recorded when the system is exposed to different excitation. The peak response amplitude operator of the roll motion of a vessel under a 90∘ incident wave is found to decrease by 26% due to the underwater structures of the DSM system. Under excitation containing irregular waves, the maximum response value occurs at 0.4 Hz in the y-axis moments under current only excitation and at 0.11 Hz in the axial force. The experiments give insight into the vessel-motion-induced vortex-induced vibration (VIV) on the rigid pipe, and find that the interaction of irregular waves and currents on the DSM system resulting in 48%, 25% and 37.8% increase of the buffer's displacements in x-, y- and z-direction compared with the linear combination of results under current only and wave only case. These results can be used to develop general guidelines for the design of DSM systems in the industry.

2) **Wave force reduction due to burial of submarine pipeline: A probability based analysis and comparison with DNVGL-RP-F109**
Neelamani, S., Al-Khaldi, M.S. 2022 Ocean Engineering 247,110786

Abstract
Horizontal and vertical wave forces were assessed on submarine pipeline for different burial depths in soils of four different hydraulic conductivities in random waves of wide range of wave height and periods. Probability analysis is carried out for 99.99% and 98% probability of non-exceedance of vertical and horizontal wave forces on the pipeline. The force reduction due to burial of the pipelines are compared with the recommendations by DNVGL-RP-F109. The effect of changing the wave height, wave period and hydraulic conductivity on the wave forces and its change due to different burial depths are revealed. The wave force values and the quantitative differences due to 99.99% and 98% probability of non-exceedance can be used for risk-based design of buried pipelines. The recommended value of wave force reduction factor for different relative burial depth of the pipeline by DNVGL-RP-F109 is much smaller than the value of wave force reduction factor from the present study. Strong scope exists to revise this code for the betterment of submarine pipeline design engineers. The knowhow revealed in this study will be useful for optimal design of buried submarine pipelines.

3) **Multi-field coupling nonlinear vibration characteristics of hydraulic lifting pipe in deep-ocean mining**

Liu, J., Zeng, L., Guo, X., Wang, P., Dai, L. 2022 Applied Ocean Research 120,103074

Abstract

To address the problem of flow-induced vibration failure of lifting pipe in deep-ocean hydraulic mining, a multi-field coupling nonlinear vibration model of deep-ocean mining lifting pipe was established by using finite element method, energy method and Hamiltonian variational principle. The longitudinal-lateral coupling effect, external current vortex-induced effect and internal fluid pulsation effect were considered, and the numerical solution of the nonlinear vibration model of lifting pipe was realized with the Newmark-β method, Newton Raphson method and finite volume method. Using the same structural parameters, the correctness and effectiveness of the proposed model were verified by comparing with the simulated experimental measurement data in the literature. On this basis, the influence of the buffer station mass and wave parameter on the vibration response characteristics and nonlinear behavior of the lifting pipe were explored. The results show that the vibration frequency of the lifting pipe near the upper end is higher, and the vibration of the pipe string near the lower end is chaotic. With the increase of the buffer station mass, the in-line flow offset and root mean square stress of the lifting pipe decrease, and the axial force on its top end is greater. Under the higher mass of buffer station, the longitudinal vibration of the lifting pipe tends to quasi-periodic motion of the ring, but the vibration amplitude is larger. Small period and large amplitude waves have obvious influences on the vibration, stress and top axial force of the lifting pipe, and make its longitudinal vibration gradually transition from chaotic motion to quasi-periodic motion.

4) **Numerical study on hydrodynamic load and vibration of pipeline exerted by submarine debris flow**

Zhao, E., Dong, Y., Tang, Y., Cui, L. 2021 Ocean Engineering 239,109754

Abstract

Submarine debris flow, as one of the natural phenomena of marine disasters, often occurs in different sea areas, which has a strong impact on marine structure due to its large specific gravity and high velocity. Submarine pipeline is an important submarine structure which is extremely vulnerable to the marine environment, especially under the submarine debris flow. Many studies have been conducted on the interaction between the debris flow and the pipeline. Based on previous studies, the effects of the debris flows under the water-air interface on the pipeline with degree of freedom are investigated in this study where the debris flow volume, density, slide slope angle, the spring stiffness coefficient, pipeline location and tandem pipeline are considered. According to the computational fluid dynamics theory, a numerical tank is established using the Immersed Boundary (IB) method, in which the three-phase media (air,

water and debris flow) are embedded. The results demonstrate that when the debris flow occurs, the water-air free surface is affected by the debris flow propagation, generating a surface wave. When the debris flow passes through the pipeline, with the increase of debris flow density and volume, the force on the pipeline increases, but the vibration frequency of pipeline decreases. Meanwhile, the vibrating pipeline will cause strong turbulence to the debris flow. In addition, the force and the vibration frequency of the pipeline are closely related to the flow pattern of debris flow reaching the pipeline. When the debris flow passes through the tandem pipeline, the closer the distance between the two pipelines is, the more significant the mutual influence between two pipelines is, because the negative pressure area formed behind the upstream pipeline can affect the downstream pipeline to a certain extent.

5) **Numerical investigation of hydrodynamic characteristics and local scour mechanism around submarine pipelines under joint effect of solitary waves and currents**
Zhao, E., Dong, Y., Tang, Y., Sun, J. 2021 Ocean Engineering
222,108553

Abstract
Submarine pipelines, as an important tool for oil and gas transportation, have been distributed in offshore oil and gas fields worldwide. Under extreme waves, a large number of submarine pipelines have been damaged in the past decades. In order to investigate the effect of extreme marine environments on the pipelines, the joint effect of solitary waves and background currents on the pipelines is numerically studied in this paper by using a numerical wave tank developed with a free surface tracking approach and the immersed boundary method. The sediment transport module including packed and suspended sediment is incorporated with the flow module. In order to ensure the calculation accuracy of this model, three verification cases related to the wave propagation profile, the hydrodynamic force on the cylinder and the scour hole profile are simulated and the numerical results match the experimental and analytical results well. Given the combined wave exerts on the different pipelines, the environmental variables consider the background current velocity and wave height, and the pipeline arrangement includes the different diameters and the suspended pipeline and tandem pipeline. It is noted that the hydrodynamic characteristics, the forces and the local scour around the pipeline are closely related to the background current and the diameter and layout of the pipeline. It is anticipated that the findings in this paper will enhance our understanding of the damage mechanism of submarine pipeline by waves and may also be useful in future design practices for pipelines.

6) **Fatigue Failure Analysis and Simulation Calculation of Submarine Suspended Pipelines**
Xu, S., Xie, X., Huang, H. 2021 Oceans Conference Record (IEEE)
2021-September

Abstract
Under the combined action of sea current and wave force in the suspended section of submarine pipelines, the stress state changes greatly, and fatigue failure is very prone to occur. Based on

actual data, this paper establishes a simulation model of the suspended section undersea conditions to explore the stress and fatigue effects of the suspended section. Mainly use the finite element software ANSYS WORKBENCH. The actual engineering is used as the research background to establish a three-dimensional nonlinear finite element model of the interaction between the submarine pipeline and the soil. Under different working conditions, carry out suspended section and stress analysis. Discuss the impact of different factors on the life of subsea pipelines. The emphasis is on the study of whether the vortex-induced resonance effect occurs in the suspended section and the fatigue damage analysis of the submarine pipeline through the two-way fluid-solid coupling. Finally, through data analysis, the stress state and fatigue of the submarine pipeline can be obtained.

7) **Software for submarine pipeline free-spanning assessment and evaluation**
Gullaksen, J. ,2021 SNAME Maritime Convention 2021, SMC 2021

Abstract

Free-spanning pipelines is a phenomenon occurring on uneven seabed and scouring phenomena around the exposed pipeline. To study how free-spanning pipelines are affected from these phenomena, it is necessary to study environmental hydrodynamic flow conditions surrounding the pipeline, such as steady flow due to current, oscillatory flow due to waves and combined flow due to current and waves. Combined wave and current loading include the long-term current velocity distribution, short-term and long-term description of wave-induced flow velocity amplitude and period of oscillating flow at the pipe level and return period values. The bending stresses and associated fatigue life are determined from the given span length and boundary conditions accounting for bending due to self-weight and environmental loading from combined direct wave action and vortex induced vibrations (VIV). The fatigue damage is calculated and integrated over all selected directions, corresponding long-term sea-states and current. Fatigue life is calculated for the in-line response model, in-line force model and the cross-flow response model. The design fatigue life for the in-line mode is a combination of the response model and the force model. Peak dynamic stresses are found from the extreme wave and current conditions and are calculated for cross-flow and in-line response. The premises for this paper are based on application development within pipeline free span evaluation in a software development project based on DNVGL recommended practice, DNVGL-RP-F105. It provides a brief introduction to a software application used to calculate parameters addressing how free-spanning pipelines are affected considering stresses, damage and fatigue life.

8) **Effect of opening and wall boundaries on CFD modeling for submarine landslide-ambient water-pipeline interaction**
Guo, X., Stoesser, T., Zhang, C., Fu, C., Nian, T. 2022 Applied Ocean Research 126,103266

Abstract

Submarine landslide-ambient water-pipeline interactions are receiving extensive attention in ocean engineering, especially the impact forces caused by landslides on pipelines.

Computational fluid dynamics (CFD) approaches are widely used to obtain these forces; however, as necessary definite solution conditions, the boundary conditions of CFD modeling are challenging to reasonably determine. In this study, the relationship between the finite volume method (FVM) in CFD modeling and boundary conditions is presented, and a classic physical flume experiment is reproduced using CFD modeling, verifying the effectiveness of the established modeling. The quantitative effect of the opening and free slip wall boundaries under variable complex working conditions (i.e., Reynolds number, pipeline span height, landslide impact velocity, and landslide rheological model) is explored via a general geometry model. The evolution characteristics of impact forces on pipelines under different boundary conditions are given. The mechanism caused by impact force changes is explained through the distributions of the velocity field, pressure field and streamlines around pipelines. Furthermore, a method for determining boundary conditions is briefly proposed, providing a basis for optimizing the CFD modeling of submarine landslide-ambient water-pipeline interactions.

9) The coastal state obligation not to impede the laying or maintenance of submarine pipelines on the continental shelf according to United Nations convention on the law of the sea

Kamiński, T., Szewczyk, R. 2022 Marine Policy
143,105086

Abstract
The exploitation of submarine cables and pipelines, notwithstanding its transboundary character, has become an inseparable element of the world economy over the last century. However, this maritime activity is associated with a high risk, and accidentally occurring events. Both may supervene as caused by human venture and natural factors, that may lead to damage to seabed pipelines or weaken their structure, which subsequently may threaten the safety of the marine environment. Suffice it to say that the intermission of the pipeline could lead to an environmental disaster comparable to the consequences of an oil spill in case of the 2010 Gulf of Mexico oil rig fire. The 1982 UN Convention on the Law of the Sea (UNCLOS), among the freedoms of the high seas mentioned in Article 87 refers to, inter alia, the freedom to lay submarine cables and pipelines. In addition, however, under article 112, UNCLOS states that this principle is fully applicable to those areas of the seas that extend beyond the outer limits of the continental shelf established by Coastal States. However, on the shelf itself this freedom is limited by the Coastal State's right under Article 79(2) of the UNCLOS to use reasonable measures to explore and exploit the shelf's natural resources and to prevent, reduce and control pipeline pollution. The next paragraph of the above mentioned article 79 also requires the consent of the Coastal state to route the pipeline whereas the last paragraph, requires the States concerned to pay due regard to the laying and maintenance of pipelines. This article is putting forward the analyzes of the scope of the indicated in UNCLOS regulations, based on the work of the UN International Law Commission, as well as documentation of the 1st and 3rd conferences on the law of the sea, in reference to the practice of states and the judgments of international tribunals. The article also refers to the theories

presented in the contemporary doctrine on the subject. The core of the considerations contained in this article is a comprehensive approach to the concept of reasonable measures, and the way of interpreting Article 79 of UNCLOS. that comes along with it.

10) Effects of siltation and desiltation on the wave-induced stability of foundation trench of immersed tunnel

Chen, W., Huang, L., Wang, D., (...), Xu, L., Ding, Z. 2022 Soil Dynamics and Earthquake Engineering 160,107360

Abstract

The evaluation of stability for the submarine artificial slope is important in the construction of offshore structures such as immersed tunnels and embedded pipelines. The siltation in marine dynamic environment is common, inevitable, but difficult to deal with. Cohesive sediment, or mud, is encountered in most water bodies throughout the world, and thus siltation inevitably occurs in the stage of underwater excavation for the offshore structure foundations. To this end, based on the temporal and spatial variations law of siltation observed from the trial trench in-situ test of Shenzhen-Zhongshan Link in China, a numerical study is carried out on the influences of siltation and desiltation on the stability of foundation trench slope under wave action. The waves are simulated by the Reynolds-Averaged Navier-Stokes (RANS) equations and then applied on the surface of seabed and trench slope. The pore pressure induced by the wave action is obtained by Darcy's law. The seabed is characterized by Mohr-Coulomb constitutive model and the factor of stability (FOS) of the slope is calculated using the strength reduction method. Three failure modes are assumed to analyze the stability of trench slope and to determine the most unstable mode. A sensitivity analysis is conducted on various key factors affecting the whole stability of the trench slope after siltation or desiltation, which is valuable for practical engineering design.

Featured Article

Numerical Study on the Hydrodynamic Characteristics of Submarine Pipelines under the Impact of Real-World Tsunami-Like Waves

by Enjin Zhao 1,2ORCID, Ke Qu 3, Lin Mu 1,2,*,Simon Kraatz 4ORCID andBing Shi 5

1 College of Marine Science and Technology, China University of Geosciences, Wuhan 430074, China

2 Shenzhen Research Institute, China University of Geosciences, Shenzhen 518057, China

3 School of Hydraulic Engineering, Changsha University of Science & Technology, Changsha 410114, China

4 Department of Civil and Environmental Engineering, University of New Hampshire, Durham, NH 03824, USA

5 College of Engineering, Ocean University of China, Qingdao 266100, China

Author to whom correspondence should be addressed.

Water 2019, 11(2), 221; https://doi.org/10.3390/w11020221

Received: 26 December 2018 / Revised: 21 January 2019 / Accepted: 22 January 2019 / Published: 29 January 2019

(This article belongs to the Special Issue Wave-structure Interaction Processes in Coastal Engineering)

Abstract

Submarine pipelines have been extensively used for marine oil and gas extraction due to their high efficiency, safety, and low price. However, submarine pipelines are vulnerable to extreme waves (i.e., tsunami waves). Previous research has often used solitary waves as a basis for studying the impacts of tsunami waves on submarine pipelines, although the hydrodynamic characteristics and wave properties drastically differ from those of real-world tsunami waves. This paper numerically investigates the hydrodynamic characteristics of tsunami waves interacting with submarine pipelines, but instead uses an improved wave model to generate a tsunami-like wave that more closely resembles those encountered in the real-world. The tsunami-like wave generated based on a real-world tsunami wave profile recorded during a 2011 tsunami in Japan has been applied. Given the same wave height, simulation results show that peak hydrodynamic forces of the tsunami-like wave are greater than those of the solitary wave. Meanwhile, the duration of the acting force under the tsunami-like wave is much longer than that of the solitary wave. These findings underline the basic reasons for the destructive power of tsunamis. It is also noted that the hydrodynamic forces of the pipeline under the tsunami-like wave increase with wave height, but will decrease as water depth increases. In addition to the single pipeline, the complicated hydrodynamic characteristics of pipelines in tandem arrangement have been also numerically studied. It is believed that the findings drawn from this paper can enhance our understanding of the induced forces on submarine pipelines under extreme tsunami waves.

Keywords: n-wave; tsunami–like wave; solitary wave; submarine pipeline; hydrodynamic forces

1. Introduction

Submarine pipelines have been widely used for marine oil and gas extraction owing to their high efficiency, safety, and low price. Since many submarine pipelines are laid directly on the seabed in the real marine environment, they are vulnerable to damage caused by extreme waves, currents, and their joint actions. For instance, the submarine pipelines of the Pinghu oil and gas field in East China were damaged due to fatigue fractures under joint action of waves and currents in 2000. During the Hurricane Katrina (2005), 102 submarine pipelines in the Gulf of Mexico were significantly damaged [1]. Much research has been carried out with regards to protecting submarine pipelines from devastating extreme surge and wave damage during their service periods. Tong et al. [2] presented a three-dimensional Large Eddy Simulation (LES) study on the hydrodynamics of a submarine pipeline located close to a wall impacted by current. Results showed that the drag coefficient on spanning sections of the pipeline is generally smaller than that of non-spanning sections, and due to the pressure gradient around the submarine pipeline, vortices shedding can be generated. The vortices shedding processes can cause the pipeline to vibrate [3,4]. Except for the influence of current on the pipeline, the hydrodynamic characteristics of a pipeline located near the seabed impacted by waves have also been investigated numerically or experimentally by many researchers. When the waves are irregular, those studies [5,6] showed that for the same conditions, the vibration amplitude of the pipeline impacted by an irregular wave is much larger than that of regular wave. An experimental investigation of wave impact loads on a slender horizontal cylinder has been conducted by haley et al. [7] using a

long wave flume. The results show that as the wave becomes very steep, the vector sum of the horizontal and vertical velocity components at the water surface may deviate significantly from the normal to the local water surface. Gao et al. [8] studied the wave forces on horizontal cylinder due to nonlinear focused wave groups and the secondary load cycle which occurs after the maximum wave crest passing the cylinder is observed. A numerical model was described by Chern et al. [9] that facilitates accurate predictions of the response behavior of a flexibly mounted horizontal cylinder under progressive waves. The model utilized a combination of direct forcing boundary simulation and the volume of fluid method to represent the moving body and water free surface. The results show that Reynolds number and Keulegan–Carpenter (KC) are two domination factors for the vibration of the submarine pipeline and the flow regime. Besides, Two-dimensional (2D) numerical simulations are performed to investigate free surface waves past two semi-submerged horizontal circular cylinders in tandem by Ong et al. [10]. When free surface waves pass two semi-submerged horizontal cylinders in tandem, for the cases with small spacing between the two cylinders, more prominent wave run-up and over-topping actions and larger positive force on upstream cylinder are observed as compared with that of the single cylinder case. According to the published articles, most studies considering submarine pipelines are conducted in general hydrodynamic conditions using experimental and numerical methods, such as steady uniform flow, airy wave, solitary wave, and so on. The intensities of forces impacting on the submarine pipelines under these conditions have been examined and analyzed, and the intensities are weaker than those under the tsunami wave.

In a real marine environment, extreme surges and waves induced by hurricanes or tsunamis can easily damage offshore and onshore infrastructures, especially submarine pipelines. To investigate the hydrodynamic characteristics of marine infrastructure subjected to tsunamis, the solitary wave has been widely used as the typical tsunami wave model since 1970s for numerical investigations [11,12,13] and experimental work [14,15,16]. For example, Francesco et al. [17] carried out the experimental and numerical investigations about the horizontal and vertical hydrodynamic forces induced by solitary waves on a horizontal circular cylinder placed on the half water depth. Small-scale laboratory tests have been performed in a wave flume and a diffusive weakly-compressible SPH model including a packing algorithm and a procedure was adopted. On the basis of the experimental and SPH results, the peaks and the shapes of the total wave forces in both directions are largely influenced by the inertia components in the present flow regime. Despite the widespread use of solitary wave, field observation, numerical simulation and experimental studies have shown that there are substantial differences between tsunami and solitary waves, such as wave profile and period [18]. Madsen et al. [19] pointed out that the required evolutionary distance for an initial free surface hump into a solitary wave far exceeds the width of any ocean on Earth and that real-world large-scale tsunamis would not evolve into solitary waves on geophysical scale. Based on the real-world tsunami profile recorded during the Tohoku tsunami event [20], tsunami waves were found to have significantly longer wavelengths than that of solitary waves. Qu et al. [21] carried out a detailed comparison between tsunami and solitary waves. It turned out that the tsunami wave produced a higher run-up distance than a solitary wave, making tsunami waves more dangerous and devastating.

Two other recent studies [22,23] investigated the tsunami induced forces on coastal structures via the use of both solitary waves and more realistic bores, and significant differences were revealed between the forces caused by two wave types. In particular, Leschka and Oumeraci [22] investigated the forces

on three vertical cylinders with different distances and arrangements using a 3D RANS numerical model. The results showed that the two wave types introduce different wave heights in the vicinity of the cylinders and different magnitude and distribution of velocities. This in turn caused differences in the forces, which in the case of solitary waves were affected by the type of the cylinder arrangement and the distance between the cylinders, while in the case of bores, the forces were dominated by the arrangement type. Istrati et al. [23] presented a comprehensive analysis of data obtained during large-scale hydrodynamic experiments of tsunami waves impacting an I-girder bridge with cross-frames. The results showed that the bores introduced a short-duration impulsive horizontal force at the instant that the wave impacted the offshore girder, which always maximized the total horizontal force, followed by a force with smaller magnitude and longer duration as the wave flooded the chambers of the deck. However, this was not the case for solitary waves. Moreover, the study developed tsunami demand diagrams, which revealed significant differences in the patterns of horizontal and vertical forces, as well as the overturning moment between the unbroken solitary waves and bores. In general, previous research studies are indicating that the solitary wave is not a suitable wave model to study the hydrodynamic characteristics of tsunamis and their interaction with coastal infrastructure.

This paper numerically investigates the hydrodynamic characteristics of submarine pipelines impacted by tsunami waves using the real-world tsunami wave profile recorded at Iwate South station during Tohoku. The tsunami wave profile is approximated using a combination of three sech2(*) wave profiles. The effects of prominent factors such as wave height, water depth, pipeline diameter, and gap-ratio on the hydrodynamic characteristics of submarine pipelines are discussed in detail. Hydrodynamic characteristics of pipelines in a tandem arrangement are also investigated. The paper is organized as follows: Section 2 describes governing equations and numerical methods; Section 3 describes the model validation; Section 4 presents the results and discussions; Section 5 summarizes the findings.

2. Numerical Model

2.1. Governing Equations

In the numerical simulation, the governing equations for incompressible flows are the three-dimensional Reynolds Averaged Navier–Stokes equations. The continuity equation in the vector form can be expressed as

$$\nabla \cdot U = 0 \tag{1}$$

The momentum equation for incompressible flow can be written as

$$\partial \rho U \partial t + \nabla \cdot (\rho U U) = \nabla U \cdot (\nabla \mu e) + \nabla \cdot (\mu e \nabla U) - \nabla p + (\rho - \rho r) \cdot g \tag{2}$$

where ∇ is the gradient operator, **U** is the flow velocity vector, ρ is the mixture density of air–water, t is the time, μ_e is the effective viscosity, ρ_r is the reference density, p is the pressure, and **g** is the gravity acceleration [24].

The k-ω model is used as the turbulence closure.

$$\partial\partial t(\rho k)+\partial\partial x_i(\rho k u_i)=\partial\partial x_j(\Gamma_k\partial k\partial x_j)+G_k-Y_k+S_k \quad (3)$$

$$\partial\partial t(\rho\omega)+\partial\partial x_i(\rho\omega u_i)=\partial\partial x_j(\Gamma_\omega\partial\omega\partial x_j)+G_\omega-Y_\omega+S_\omega \quad (4)$$

where Γ_k and Γ_ω represent the effective diffusivity of k and ω, respectively. G_k represents the generation of turbulence kinetic energy, G_ω represents the generation of ω, Y_k, and Y_ω represent the dissipation of k and ω, S_k and S_ω are source terms. In the simulation, the k-ω model is used as the turbulence closure due to two reasons. Firstly, the simulation and calculation of the fluid nearby the wall are more stable using this turbulence model than other models. In order to capture the detailed flow around the wall of submarine pipeline, this turbulent closure is selected. Secondly, the calculation accuracy of the model can be ensured when the counter-pressure gradient flow is simulated. So, this turbulent closure is suitable for the solution of free shear turbulence flow, boundary layer turbulence flow, and moderate separation turbulence flow when the wave passes the submarine pipeline.

In the model, the transportation equation of the volume of fluid (VOF) method is written as

$$\partial\gamma\partial t+\nabla\cdot(\gamma U)=0 \quad (5)$$

The local density and laminar viscosity of every mesh grid are defined by volume fraction γ, which is adopted to capture the free surface between water and air for the generation and propagation of wave.

$$\rho=\rho_{air}+\gamma\cdot(\rho_{water}-\rho_{air}) \quad (6)$$

$$\mu_l=\mu_{air}+\gamma\cdot(\mu_{water}-\mu_{air}) \quad (7)$$

$$\gamma=\begin{cases}\\ \\ \end{cases}\gamma=00<\gamma<1\gamma=1,,,\begin{matrix}air\\interface\\water\end{matrix} \quad (8)$$

In the model, the collocated finite volume method is implemented to discretize the continuity and momentum equations, and the deferred correction is employed to discretize the convective terms by combining the first-order upwind scheme and the second-order Gamma scheme. In order to couple the continuity and momentum equations, the momentum interpolation method is adopted to interpolate the velocities of the control cell centers to the control cell faces [25]. And then the velocities and pressures are resolved by the Pressure Implicit Split Operator (PISO) method. The sharpness of the free surface between the water and air is controlled by the Switching Technique for Advection and Capturing of Surfaces (STACS).

2.2. Wave Generation Method

A piston-type wave maker is simulated using the dynamic mesh technology, as shown in **Figure 1**. In hexahedral mesh zone, the layer height (H_i) is specified on moving boundary firstly. Based on the height, the layer of cells (layer j) adjacent to the moving boundary is split or merged with the layer of cells (layer i) next to it. The dynamic layering mesh adjacent to moving boundary is added or removed layers of cells. To produce the desired free surface profile, the position of the moving boundary changes with time [26,27]. Solitary and tsunami waves are generated using the piston-type wave maker depending on the following methods.

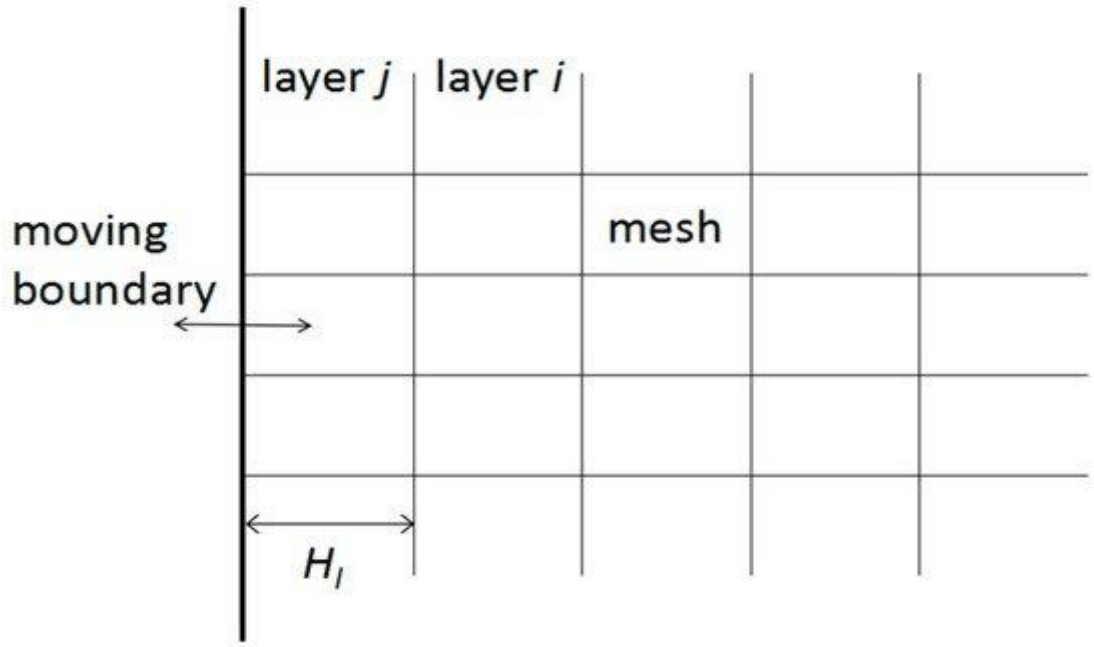

Figure 1. Dynamic layers of moving boundary.

The wave elevation of the solitary wave with a constant water depth h can be written as

$$\eta(x_i,t)=H_o\mathrm{sech}^2[k_o(x-x_o-C_oT_o)] \quad (9)$$

where H_o is the wave height, $k_o = (3H_o/4h^3)^{1/2}$ is the effective wave number, x_o is the location of the wave crest at $t = 0$, $C_o = [g(H_o + h)]^{1/2}$ represents the wave celerity, T_o is the wave period of a solitary wave which is defined by the effective wave number.

To reproduce the real-world tsunami wave, a combination of three sech ^{2}(*) wave profiles is used to model the tsunami wave based on the concept of N-wave. The combination of three sech ^{2}(*) wave can be written as

$$\eta(x_i,t)=\sum_{i=1}^{3}H_i\mathrm{sech}^2[\omega_i(t-(t_o+t_i))] \quad (10)$$

In the following sections, we name the wave profile described by Equation (10) as tsunami-like wave. To enable a general application of tsunami-like wave profile, the parameters of the tsunami-like wave presented in previous researchers [**20**,**28**] have been normalized as follows

$$(H_1H_o\omega_1\omega_ot_1T_o)=(-0.1190.08566.556)(H_2H_o\omega_2\omega_ot_2T_o)=(0.3280.09478.776)(H_3H_o\omega_3\omega_ot_3T_o)=(0.8730.3124410.54) \quad (11)$$

where ω_o is the wave frequency of a solitary wave with the same wave height as the tsunami-like wave.

To generate solitary wave and tsunami-like wave, the velocity of wave paddle can be described as

$$u=\sum_{i=1}^{3}u_i \quad (12)$$

and

$$u_i=C_i\eta_i/(h+\eta_i) \quad (13)$$

The wave profile approximated by the wave generation formula and the observed wave profile at Iwate South station during 2011 Japan tsunami event are shown in **Figure 2**.

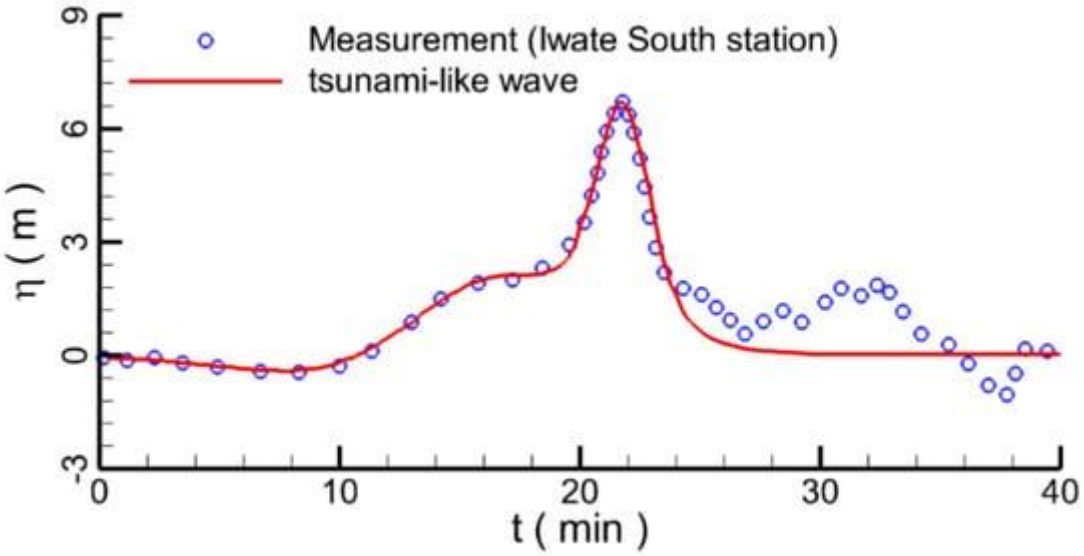

Figure 2. Comparison between the tsunami-like wave and the measured wave.

3. Model Validation

To evaluate the computational capability of our model in predicting hydrodynamic forces, solitary wave impacting the submarine pipeline is numerically investigated in this section. The corresponding experimental work was performed by Sibley [**29**]. The experimental layout is shown in **Figure 3**, where *D* is the pipe diameter and *G* is the space between the pipe and the bottom boundary. The wave height and water depth are denoted as *H* and *h*, respectively.

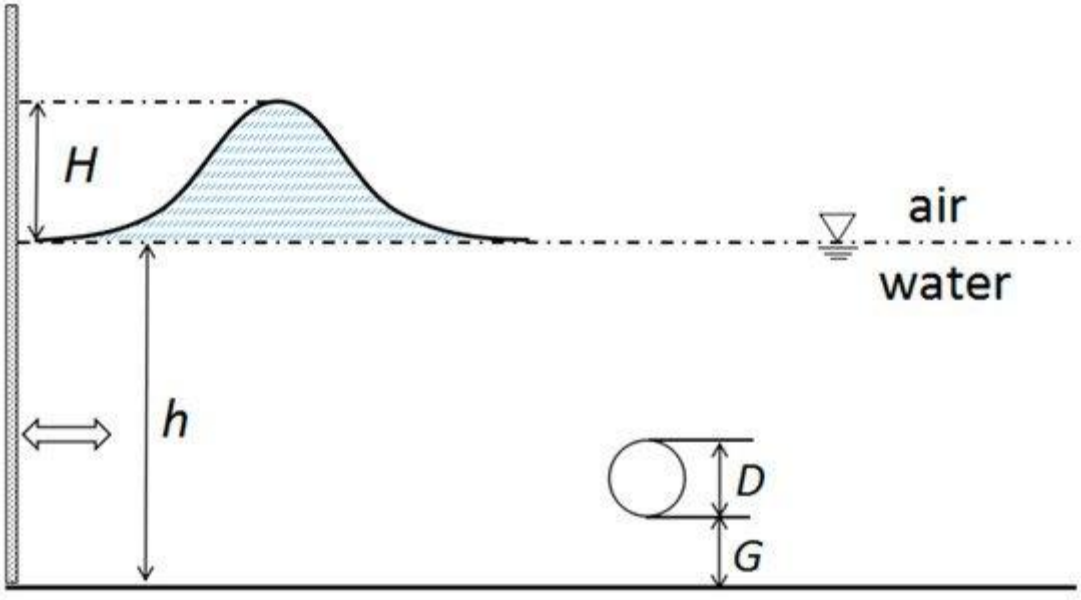

Figure 3. Schematic representation of the experimental layout.

Two experimental runs are selected using parameters provided in **Table 1**. The computational domain is 30 m in length and 0.5 m in height. The origin of the x coordinate is set at the left boundary and the origin of the z coordinate is set at the bottom boundary. The center of the circular cylinder is

located at x = 3 m. The computational mesh consists of 365,512 elements and the mesh resolution near the circular cylinder is about 0.05 mm. To meet the mesh resolution requirement, another two groups of meshes have been generated: a medium and coarse mesh with 185,145 and 91,497 mesh elements, respectively.

Table 1. Parameters of selected experimental runs.

Figure 4 depicts the snapshots of the vorticity contour at different times for run 1. When the solitary wave approaches the cylinder, a pair of vortices are gradually generated at the rear side of the cylinder. Once the solitary wave passes over cylinder, vortices can be shed from the cylinder surface and complicated flow phenomena can be observed (**Figure 4**d). **Figure 5** depicts the snapshots of the vorticity contour for run 2. When the crest of the solitary wave is above the pipeline, a pair of narrow vortices are formed behind the pipeline. After vortices are shed from the cylinder, they strongly interact with the boundary layer at the seabed (**Figure 5**d).

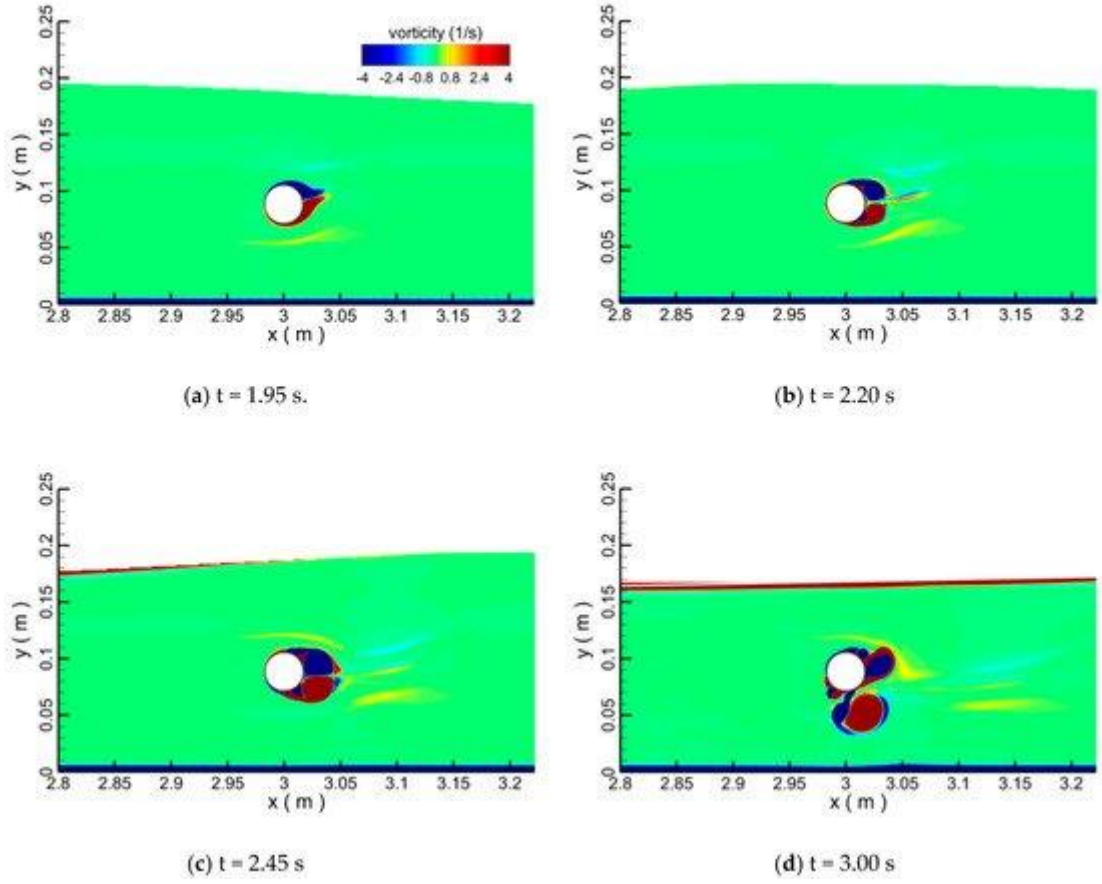

Figure 4. Snapshots of vorticity contour of the flow field at different times for run 1.

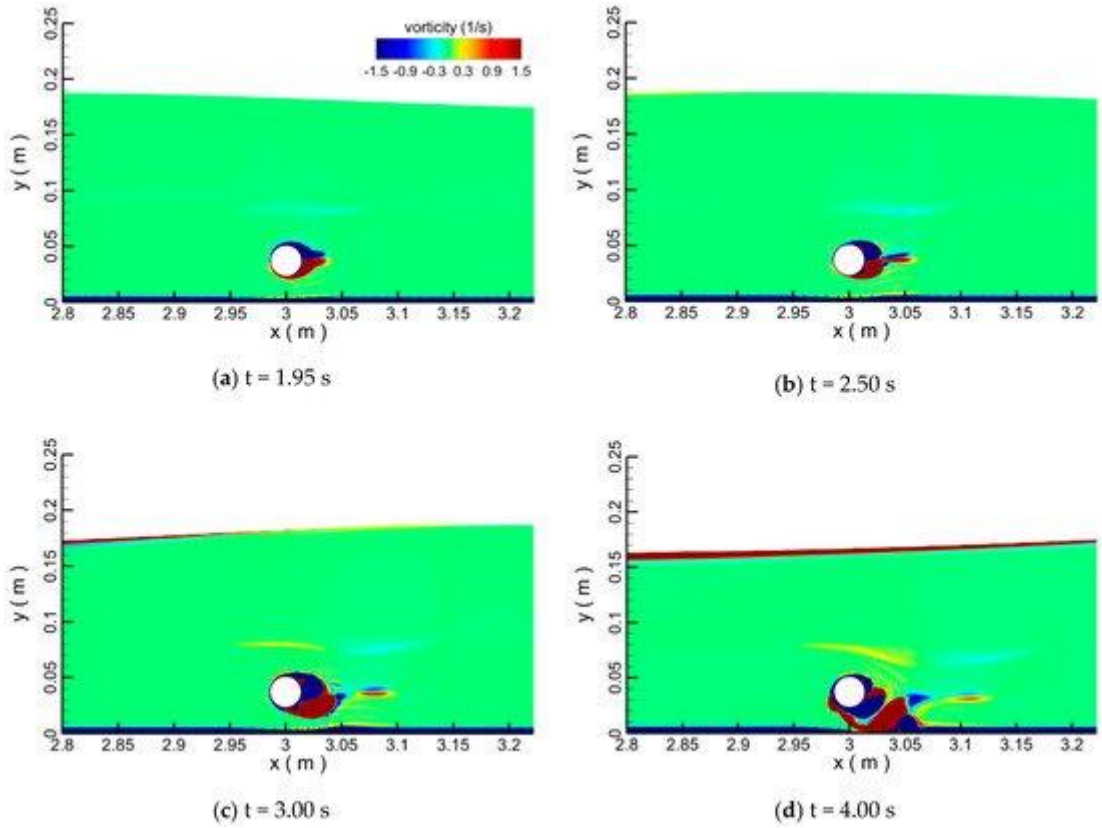

Figure 5. Same as **Figure 3** but for run 2.

Time series comparisons of the resultant hydrodynamic forces at the pipeline between measurements and numerical predictions are plotted in **Figure 6** (run 1) and **Figure 7** (run 2), where both horizontal and vertical forces are nondimensionalized by ρghA ($A = \pi D^2/4$), namely, $F^* = F/\rho ghA$. In the rest of the paper, all hydrodynamic forces are presented using this method. Predicted horizontal and vertical forces are in good agreement with corresponding measurements in both peak force values and temporal evolution process. Forces for the medium and dense meshes are nearly identical whereas those computed on the coarse mesh are noticeably different from measurement. Hence, the resolution of dense mesh and medium mesh is sufficient. In order to guarantee the calculation accuracy, a similar resolution mesh setup as dense mesh will be applied in the following simulation. By carrying out the simulation work in this section, the computational capability of our model in predicting the hydrodynamic forces of submarine pipeline is well calibrated.

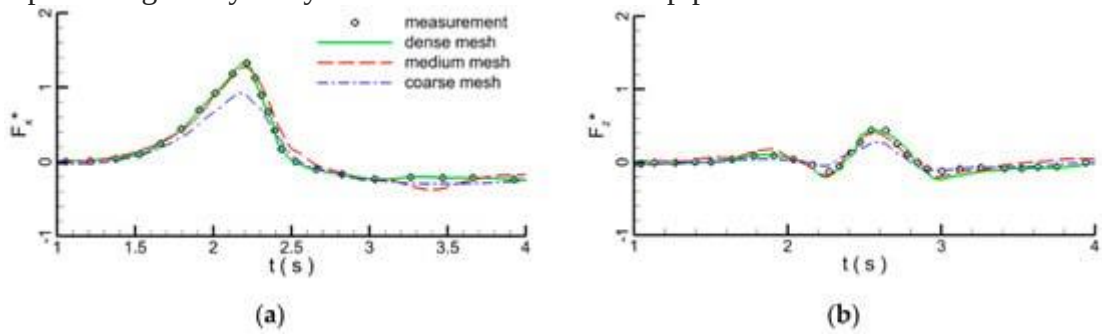

Figure 6. Force comparison between measurement and simulation in run1; (**a**) horizontal force F_x*; (**b**) vertical force F_z*.

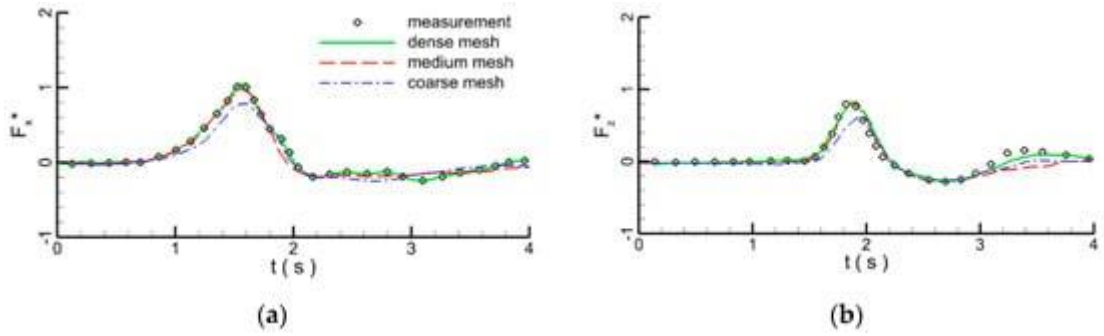

Figure 7. Force comparison between measurement and simulation in run 2; (**a**) horizontal force F_x*; (**b**) vertical force F_z*.

4. Results and Discussions

The hydrodynamic characteristics of submarine pipelines impacted by the tsunami-like wave are systematically investigated. Effects of prominent factors, such as wave height, water depth, pipeline diameter, and spacing distance between pipeline and seabed are discussed in detail. For comparison purpose, the flow field around pipelines under solitary wave conditions is also numerically simulated. In ocean engineering, many pipelines transport gas and oil in tandem, so the hydrodynamic environment around a tandem pipeline is also investigated. In this study, the marine environmental conditions are referred to the Bohai Sea in China which is the innermost gulf of the Yellow Sea and the Korea Bay on the coast of Northeastern and North of China. Many submarine pipelines are working in the Suizhong 36-1 Oil Field which is located in Liaodong Bay of Bohai Sea and the distance from this oilfield to Suizhong County is about 50 km. The sea area is relatively flat and there are not many steep slopes. Considering the marine environmental conditions in this realistic oil field, the parameters of this study are selected.

The computational domain is 2000 m in length and 20 m in height. The horizontal coordinate of the pipeline center is x = 100 m. The mesh resolution around the submarine pipeline is similar to that presented in **Section 3**. In the whole computational domain, the mixed grids are adopted where unstructured grids are around the submarine pipeline with the grid size of 0.05 m and structured grids are used in another domain. When the wave passes the pipeline, the effect of the wave on submarine pipeline becomes weaker and weaker and the mesh behind the submarine pipeline also becomes looser and looser. The scale of grid increases depending on the increase ratio of 1.2. In the whole computational domain, about 956,000 grids are used. The computational layout of the single pipeline is depicted in **Figure 8**, where P is the velocity sensor locating at (x = 50 m, z = 1 m), and L1 and L2 are the elevation sensors locating at x1 = 100 − 0.55D m and x2 = 100 + 0.55D m, respectively. The computational layout for the pipelines in tandem arrangement is shown in **Figure 9**, where S is the distance between two pipelines. The time-step size is 0.005 s, the number of time steps are 10^5 and the maximum iterations are 20. Depending on the numerical model, 2D simulations are conducted. The calculation was performed on the Dell Precision 3630 Tower, which includes 12 central processing units (CUPs). The CPU type is Intel (R) Core (TM) i7-8700 CUP @ 3.20GHz which is produced by Intel Corporation, California, America. The storage of the internal memory and hardware are 16G and 2T, respectively. In order to save computation time, four cases were run simultaneously on one computer. The real duration for one case is about 115 h. When the simulation begins, the program reads the initial boundary conditions and mesh grids. Depending on the numerical methods, the results

are generated and saved according to the storage time step. Because the moving-mesh method is used in the simulation, when the results are saved, the changed meshes are also saved.

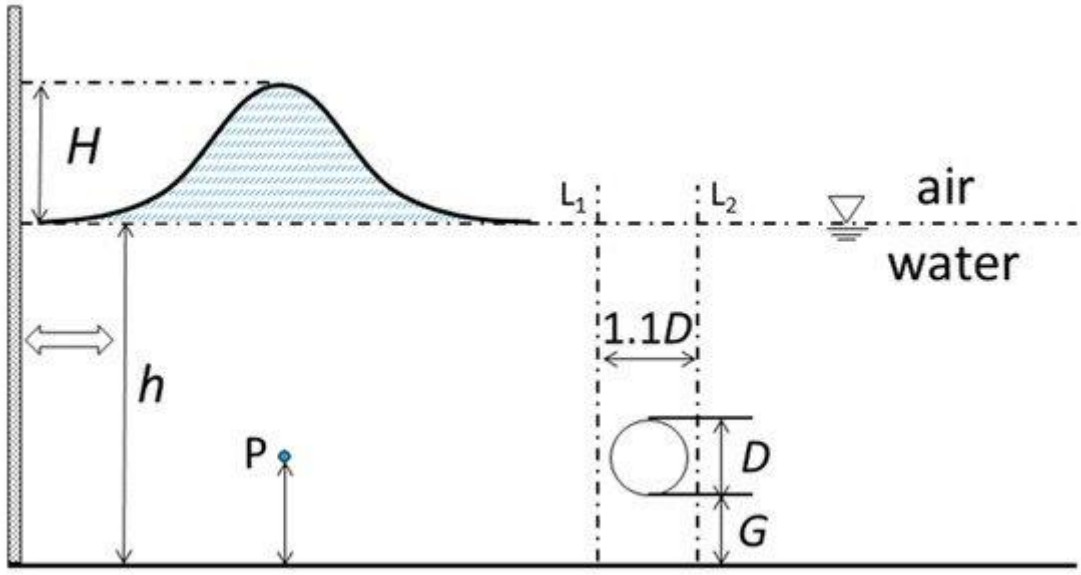

Figure 8. Computational layout for wave impacting a single submarine pipeline.

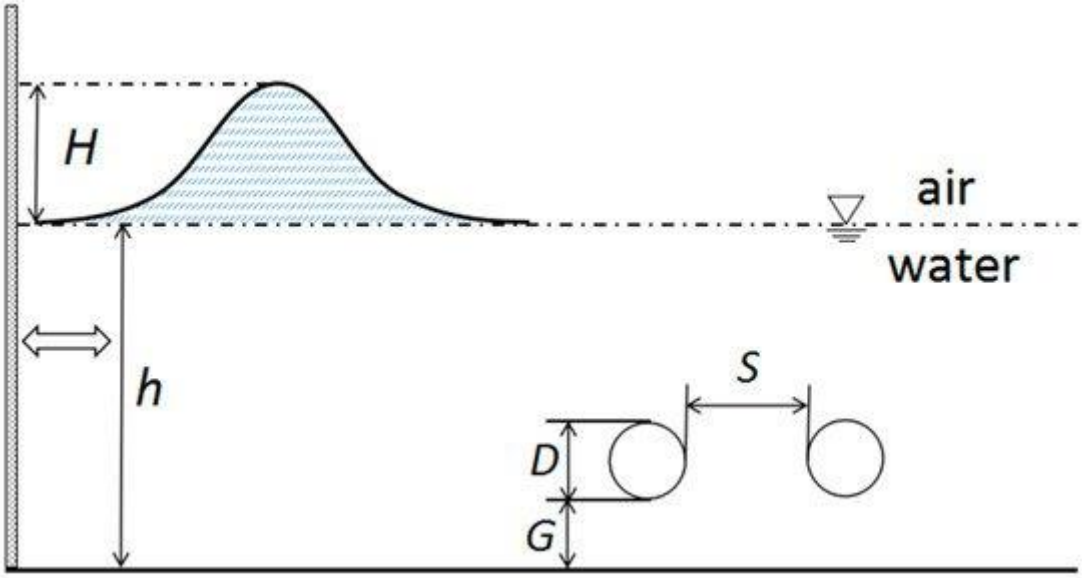

Figure 9. Computational layout for wave impacting pipelines in tandem arrangement.

4.1. Single Pipeline

In this section, a tsunami-like wave impacting single pipeline is numerically investigated. The water depth *h* and wave height *H* are 8 m and 2 m, respectively. The pipeline diameter *D* is 1 m and the pipeline is located on the seabed (*G* = 0). In the study, the submarine pipeline is laid on the seabed directly without any gap and we did not consider the gap ratio in this case. The flow cannot pass at the bottom of the submarine pipeline. The surface of the submarine pipeline connects the seawall, as shown in the small graph of **Figure 10**. The distance between the start point and the end point is about 0.02 m which is much less than the pipeline diameter of 1 m. Also, the contact between the submarine

pipeline and seabed is more realistic in ocean engineering. As for the forces, we integrated the forces distributed on the whole cylinder from the start point to the end point.

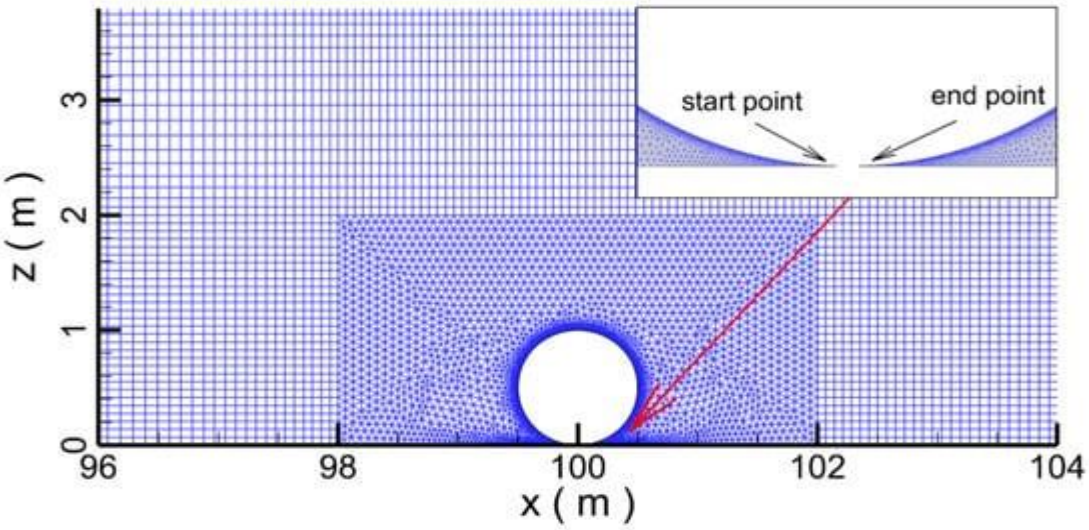

Figure 10. The mesh setup around the submarine pipeline.

In **Figure 11**, due to the movement of the boundary from the left to right, the water is compressed and the water level rises, which generates the wave. At the beginning of wave generation, the wave generation paddle is placed at x = 0, and the surface of the water remains horizontal. At 76 s, the numerical wave generation paddle moves along the x axis, pushing the water and generating the wave. At 80 s, the crest of the tsunami-like wave is created by the wave generation paddle. The shape of the tsunami-like wave can be seen in **Figure 11**d. The results suggest that when the boundary moves, the wave is generated and propagates steadily along the flume (**Figure 11**), which means this wave-making method can generate a satisfactory wave for the research.

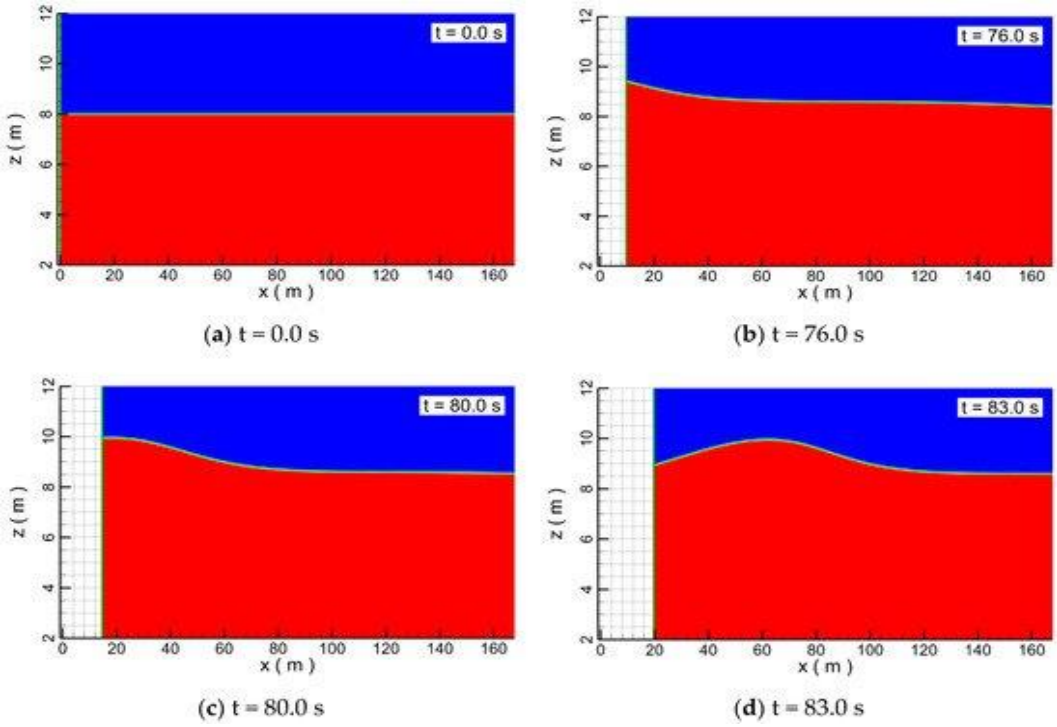

Figure 11. The wave generation process around the wave paddle.

The profiles of the tsunami-like wave and the solitary wave generated by the piston-type wave maker are displayed in **Figure 12**a and **Figure 13**a.

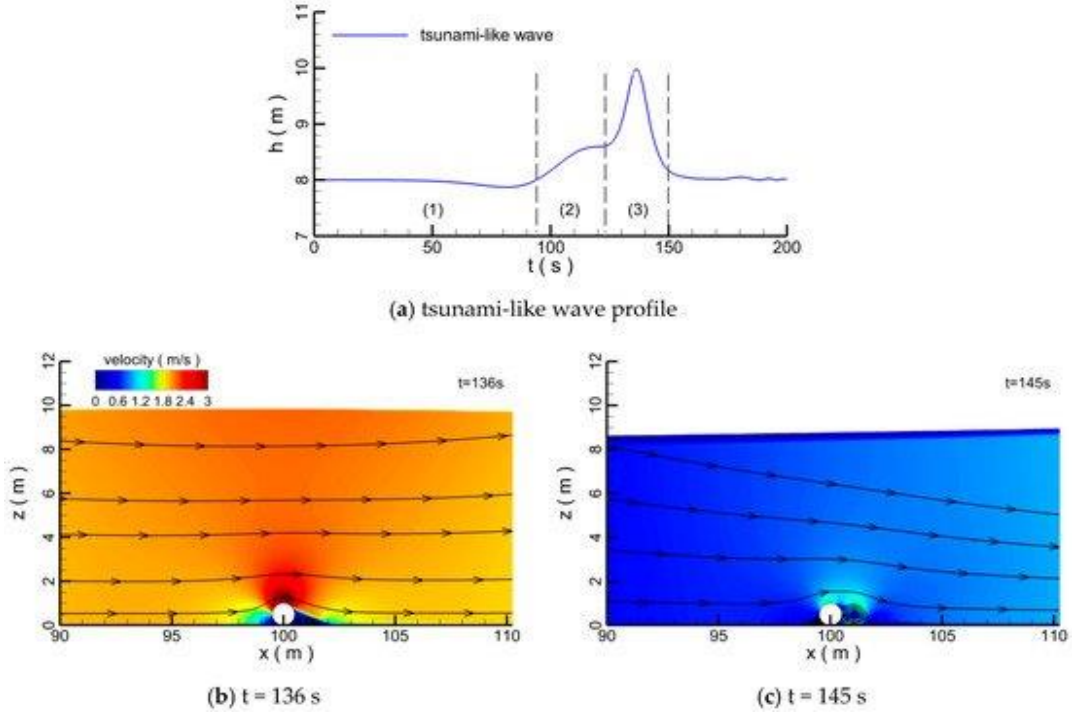

(a) tsunami-like wave profile

(b) t = 136 s

(c) t = 145 s

Figure 12. Snapshots of the velocity contour around the submarine pipeline at different times for the tsunami-like wave.

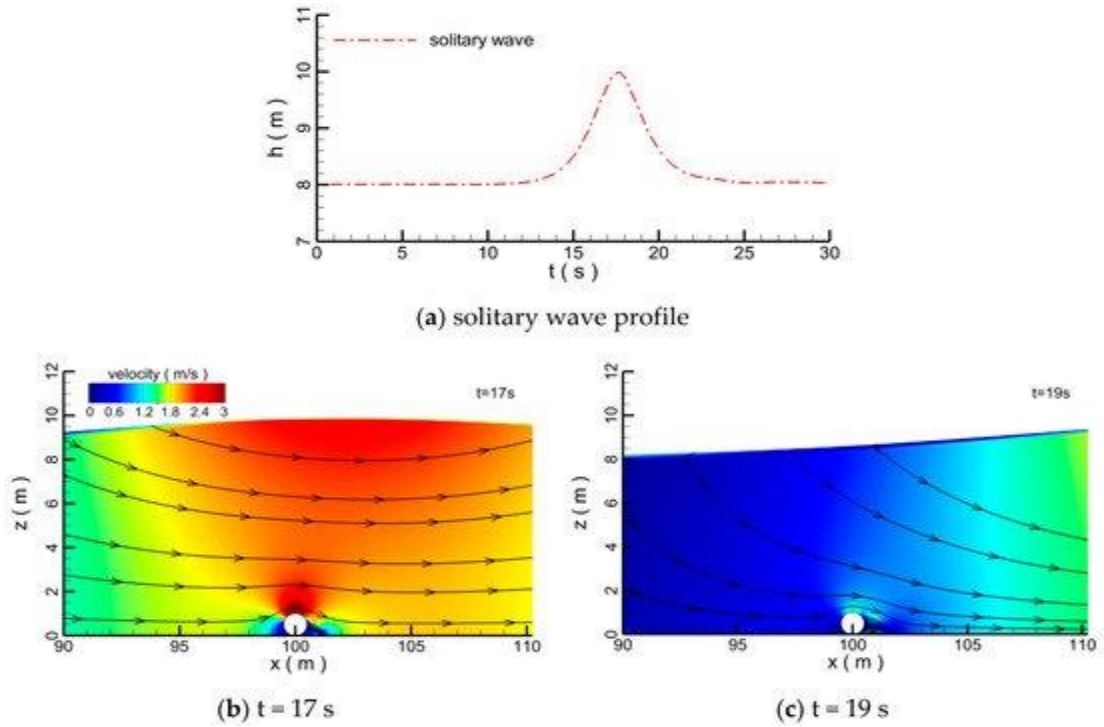

(a) solitary wave profile

(b) t = 17 s

(c) t = 19 s

Figure 13. Snapshots of the velocity contour around submarine pipeline at different times for the solitary wave.

Three parts of the tsunami-like wave can be seen:

(1) the leading-depression wave portion;

(2) the preceding elevated wave portion;

(3) the secondary elevated wave portion.

Compared with the solitary wave (**Figure 13**a), the duration of the tsunami-like wave is much longer (**Figure 10**a). As the crest of the tsunami-like wave approaches the pipeline, small vortices are gradually generated at the frontal and rear sides of pipelines (**Figure 12**). At t = 136 s, when the crest of the wave is just above the pipeline, the velocity magnitude of the flow field around the pipeline approaches its maximum and the free surface above the pipeline is rather flat (**Figure 12**b). After the tsunami-like wave passes the pipeline, the size of the vortices at the frontal and rear sides of pipeline increases substantially, even though the magnitude of the flow velocity near the pipeline decreases (**Figure 12**c). There are two main regions where the magnitude of the velocity is large when the crest of the solitary wave is located above the pipeline: the region just above the pipeline, and the region near the water surface (**Figure 13**b). Besides, the water free surface under the tsunami-like wave is gentler than that under the solitary wave, because the duration of the tsunami-like wave is longer than that of solitary wave. After the solitary wave has passed the pipeline, the vortices behind the pipeline are much smaller than for the tsunami-like wave (**Figure 12**c and **Figure 13**c).

Time series of water elevation recorded at elevation sensors L_1 and L_2 under tsunami-like wave and solitary wave conditions are depicted in **Figure 14**. Since the diameter of the pipeline is relatively small compared to still water depth, for both solitary and tsunami-like waves, the wave profiles are almost unchanged. Although the blocking effect of the pipeline on wave propagation is very weak, the crests of two waves still fluctuate slightly. The wave heights decrease for both waves when they pass through the pipeline. The wave height of the solitary wave decreases more than that of the tsunami-like wave. The difference between the two wave shapes are independent of the difference in the wave peaks due to the different scattering. The maximum velocity of the tsunami-like wave measured at P is about 1.15 times of that of the solitary wave at the same wave height (**Figure 15**). Also, the duration of the high-velocity portion is much longer for the tsunami-like wave.

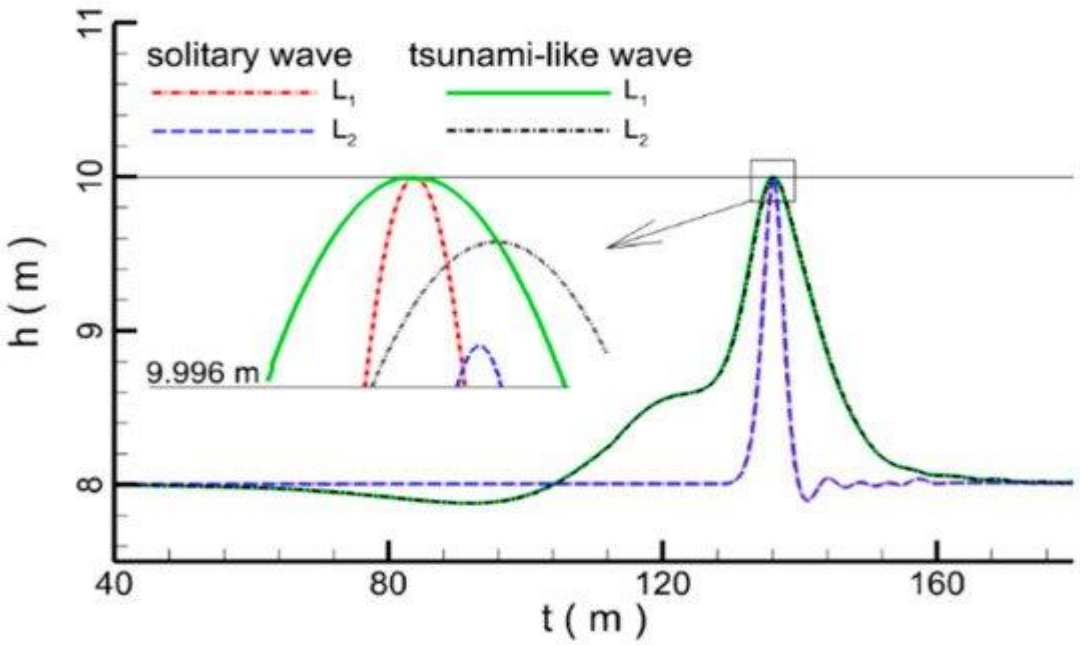

Figure 14. Time series of water elevations recorded at elevation sensors L1 and L2 for the solitary and tsunami-like wave.

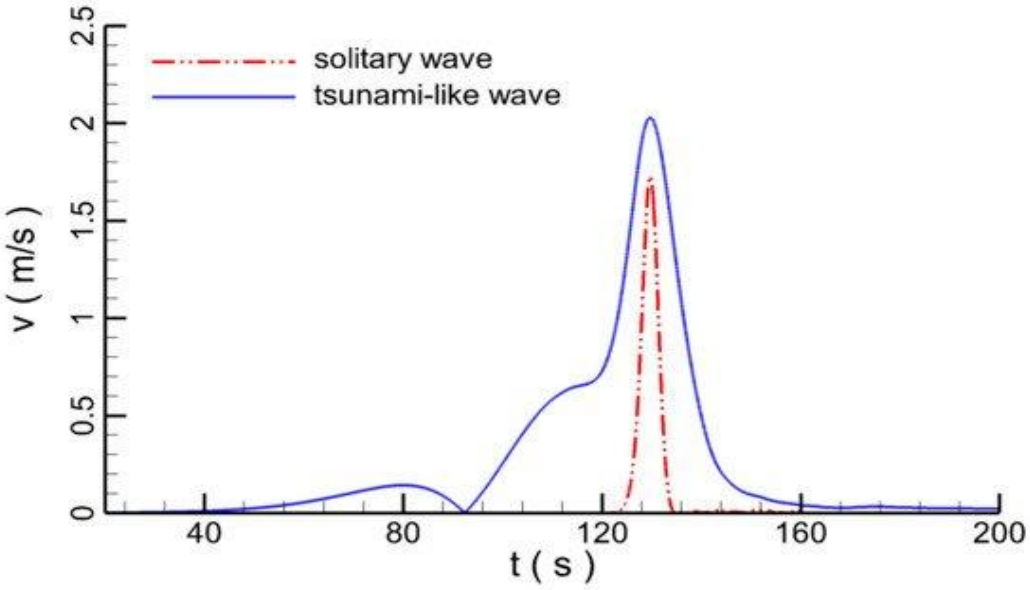

Figure 15. Time series of velocity at velocity sensor P during the tsunami-like wave and solitary wave.

The time series of the horizontal and vertical forces exerted at the pipeline when impacted by the tsunami-like and solitary waves are plotted in **Figure 16**. The horizontal and vertical forces on the cylinder are obtained from surface integration of the hydrostatic pressure, hydrodynamic pressure, and shear stresses. When the flow arrives at the submarine pipeline, due to the obstruction of the pipeline to the water body, the flow velocity reduces and flow direction changes. Correspondingly, the submarine pipeline suffers the force of the flow. The peak values of the horizontal and vertical forces

for the tsunami-like wave are larger than for the solitary wave. The horizontal force peaks for both waves are similar to each other; on the contrary, noticeable differences can be detected in the vertical forces, which are caused by two reasons. Firstly, when the wave passes the pipeline, the velocity of the tsunami-like wave is larger than that of the solitary wave. The bottom water flows from the seabed to the top of the submarine pipeline, which is mainly subjected to vertical upward force. The larger the velocity, the larger the vertical upward force. Secondly, the crest levels for two different waves are different after the waves pass through the pipeline. The vertical force includes the vertical hydrodynamic force and the hydrostatic force. The crest level of the tsunami-like wave is higher than that of the solitary wave, which also causes the vertical force under the tsunami-like wave to be larger than that of the solitary wave. However, the horizontal force only includes the hydrodynamic force which is affected by the horizontal velocity. Due to the fact that the horizontal velocities of two waves are similar to each other, the horizontal force peaks under two waves are also close. Interestingly, in the horizontal direction, the negative force also can be seen in **Figure 16**a. It is very easy to understand that when the wave passes the submarine pipeline, the horizontal flow causes the force on the submarine pipeline in normal direction due to the pressure gradient in front and to the rear of the submarine pipeline. The greater the velocity, the greater the force. However, after the wave passes the submarine pipeline, the pressure gradient does not disappear rapidly. Much water will flow to the negative pressure zone behind the submarine pipeline, which causes the water reflux. The reflux water will induce flow in the negative direction. When the negative flow acts on the submarine pipeline, negative horizontal force is generated. This is a normal phenomenon in the wave propagation for the tsunami-like and solitary wave. The pressure gradient caused by the wave determines the velocity of the water reflux. The larger the pressure gradient, the more the reflux water and the greater the negative horizontal force on the submarine pipeline. Due to the interaction between the submarine pipeline and flow, the energy contained by the flow dissipates gradually, the pressure gradient reduces, and the water finally reaches the equilibrium state. The horizontal force on the submarine pipeline reduces to zero. In general, the duration of the tsunami-like wave is longer than that of solitary wave. The duration of the acting force under the tsunami-like wave is also much longer than for the solitary wave, and the more energy is contained by the tsunami-like wave. Under the action of a tsunami-like wave, the pipeline is more like to be damaged. The presented results show that a real-world tsunami wave cannot be directly simplified to a solitary wave, and explains the reasons for the devastating power of tsunami waves due to their large impact intensity and longer duration.

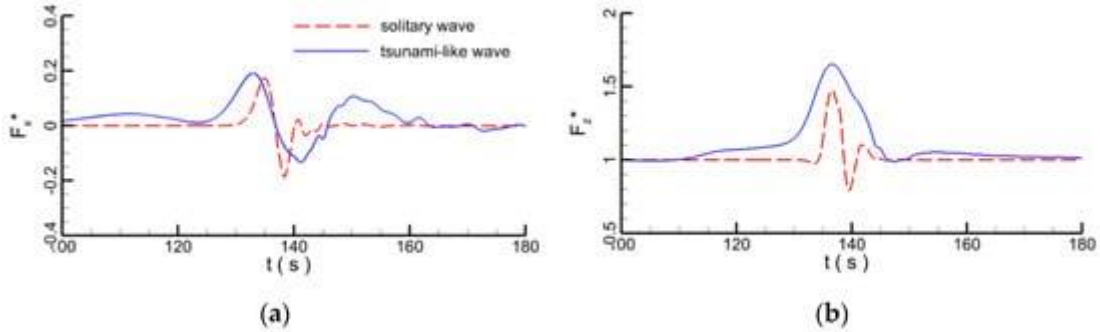

Figure 16. Time series of hydrodynamic forces at a pipeline under tsunami-like and solitary waves; (**a**) horizontal force F_x*; (**b**) vertical force F_z*.

Based on the above research, the effects of wave height, water depth, pipeline diameter, and spacing between pipeline and seabed are discussed.

4.1.1. Effect of Water Depth

This section discusses the impact of water depth on the hydrodynamic characteristics of the submarine pipeline. With a wave height H = 2 m, pipeline diameter D = 1 m, and G = 0, six different water depths are selected: 4 m, 6 m, 8 m, 10 m, 12 m, and 14 m. For comparison purposes, the time series of water elevation recorded at elevation sensor L_1 at different water depths are plotted in **Figure 17**. It is seen that the wave profile of the tsunami-like wave gradually becomes fatter and its wave period becomes longer as water depth increases, thus increasing its energy carrying capacity.

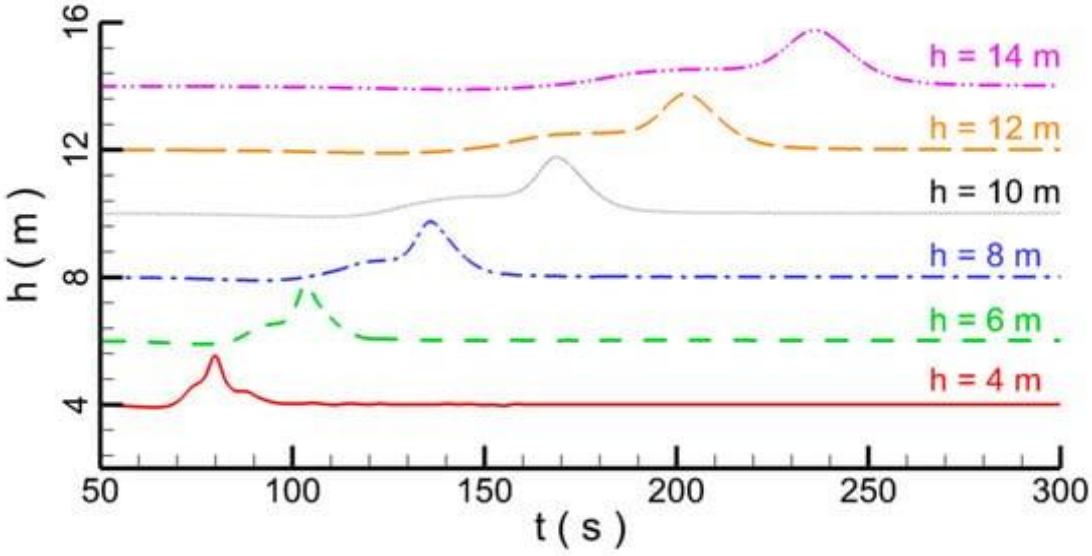

Figure 17. Time series of water elevation recorded at elevation sensor L_1 for a tsunami-like wave at different water depths.

The time series of flow velocity magnitude recorded at velocity sensor P during tsunami-like wave impacting the pipeline are displayed in **Figure 18**. When the water depth increases (**Figure 18**a), the maximum velocity decreases (**Figure 18**b). For example, when the water depth is 4 m, the maximum velocity magnitude is about 2.7 m/s, however, when the water depth is 14 m, the velocity decreases to 1.5 m/s.

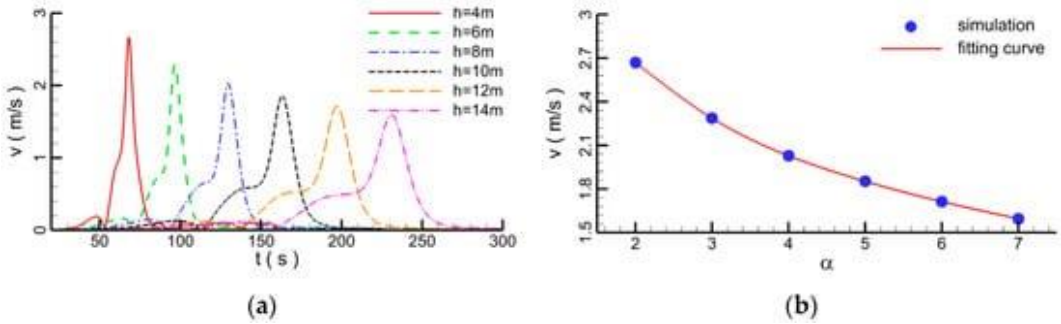

Figure 18. The variations of velocity at different water depths recorded at sensor P; (**a**) time series of velocity; (**b**) maximum velocity as function of water depth. α is the ratio of water depth h to the wave height H.

The maximums and minimums of horizontal and vertical forces as functions of water depth for the solitary and tsunami-like waves are shown in **Figure 19**. Interestingly, as water depth increases, both maximum horizontal and vertical forces decrease (**Figure 19**a,b), and the magnitude of the minimum forces decreases at the same time (**Figure 19**c,d). This is consistent with the variations of

velocity shown in **Figure 18** as water depth increases, inflow velocity in front of the pipeline decreases, and hence the resultant hydrodynamic forces also decrease. When the water depth is greater than 6 m, the maximum horizontal forces of the solitary wave and tsunami-like wave become similar. With the increase of water depth, the shoaling becomes weaker and weaker. This is the main reason why the tsunami wave is not obvious in the deep sea, but in shallow water around a beach, a tsunami-wave can cause the tremendous damage. Similarly, with the increase of water depth, the difference of maximum forces on the submarine pipeline under the tsunami wave and solitary wave becomes smaller and smaller. However, the solitary wave still cannot be used instead of a tsunami-like wave to study the effect of tsunami waves on ocean or coastal infrastructure. In some special conditions, the maximum forces under two different wave types are similar, but not the same. The duration of the acting force under the tsunami-like wave is also much longer than for the solitary wave. In other words, the energy contained by the tsunami-like wave is much greater than that of a solitary wave. Besides, the changes of the forces on the submarine pipeline under two types of wave are also completely different, which may cause the different fatigue damage to the pipelines. However, for the same wave height and water depth, the maximum hydrodynamic forces at the pipeline under solitary wave are always smaller than that of tsunami-like wave. There is a great difference between maximum force and minimum force for tsunami-like wave and solitary wave. This is because when the waves pass the submarine pipeline, the maximum force is caused by the horizontal velocity which is similar for the two different types of wave. However, the minimum force is caused by the water reflux after the wave passes the submarine pipeline. The pressure gradient around the pipeline and water volume under the tsunami-like wave are much greater than that of a solitary wave, so the effect of the water reflux under the tsunami-like wave is more serious than for a solitary wave. Compared with the maximum forces under the tsunami-like wave and solitary wave, the minimum forces are more different.

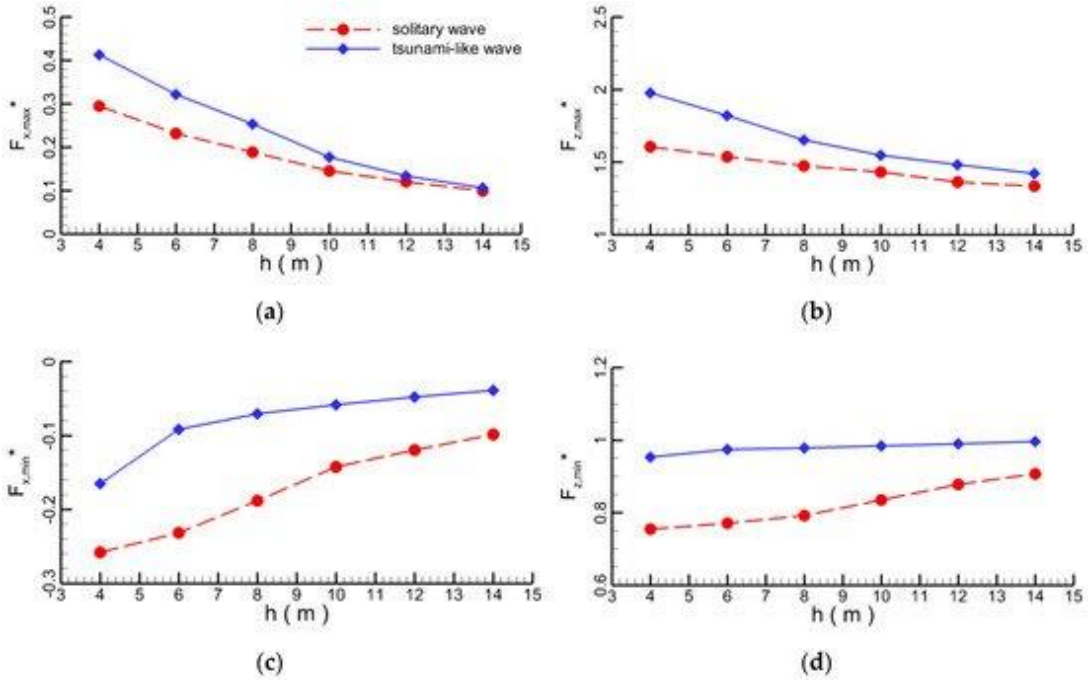

Figure 19. Plots of maximum forces as function of water depth; (**a**) maximum horizontal force $F_{x,max}$*; (**b**) maximum vertical force $F_{z,max}$*; (**c**) minimum horizontal force $F_{x,min}$*; (**d**) minimum vertical force $F_{z,min}$*.

4.1.2. Effect of Wave Height

This section numerically investigates the effect of wave height on the hydrodynamic forces at the pipeline for the tsunami-like wave. The water depth *h* is 10 m, the pipeline diameter *D* is 1 m, and it is located at the seabed (*G* = 0). Four different wave heights are selected: *H* = 1 m, 2 m, 3 m, and 4 m. The duration is largely decreasing with increasing wave height (**Figure 20**). The maximum velocity recorded at sensor P increases monotonically with wave height (**Figure 21**).

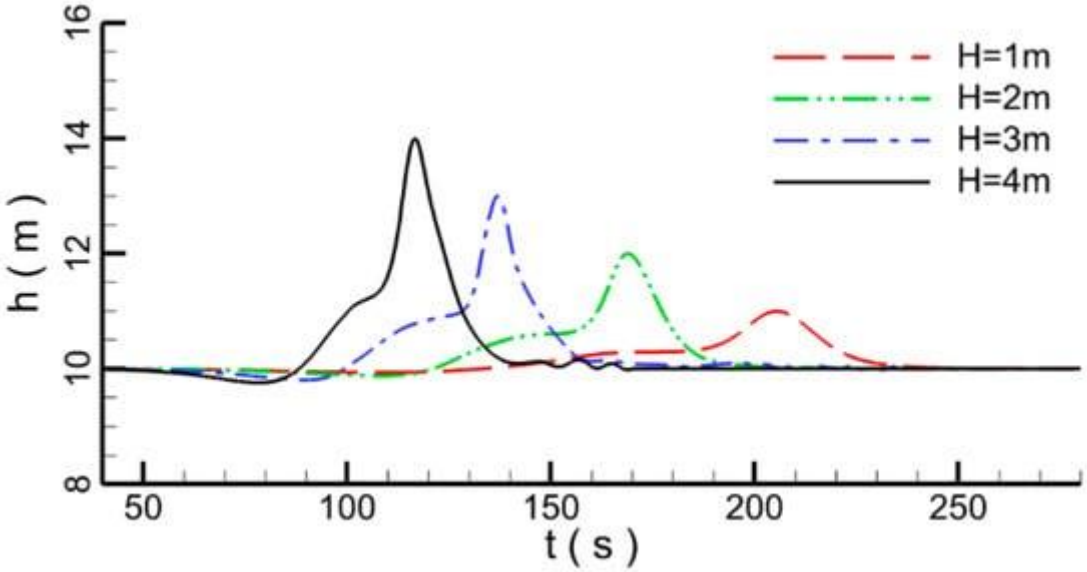

Figure 20. Time series of the tsunami-like wave profile recorded at sensor L_1.

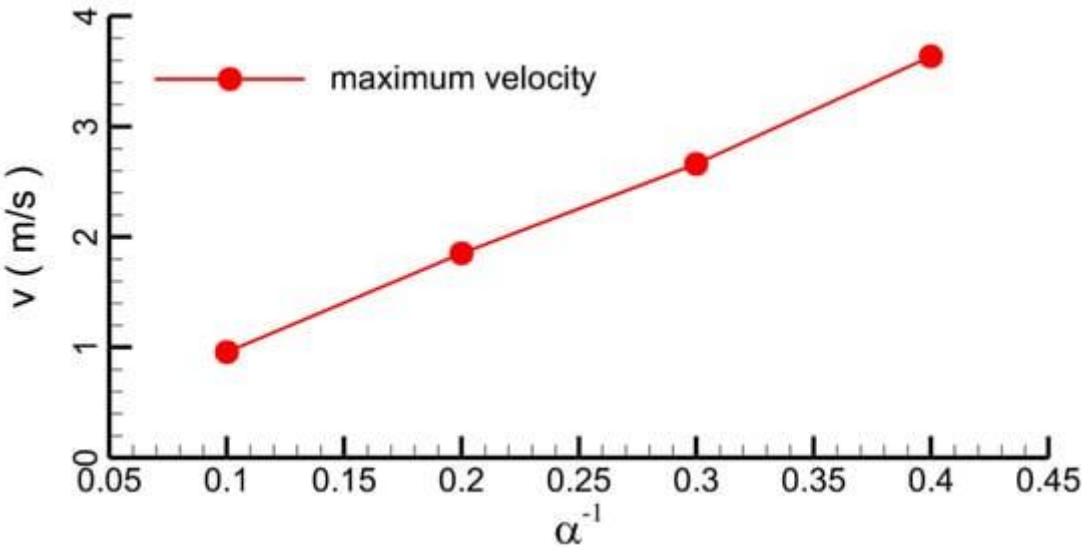

Figure 21. Plots of maximum velocity recorded at sensor P as function of wave height.

Both the maximum horizontal and vertical forces gradually increase with wave height (**Figure 22**a,b), but much more rapidly for the tsunami-like wave. This again demonstrates that the hydrodynamic characteristics of the tsunami-like wave are drastically different from that of the solitary wave. As the wave height increases, the magnitudes of the minimum horizontal and vertical forces gradually decrease (**Figure 22**c,d).

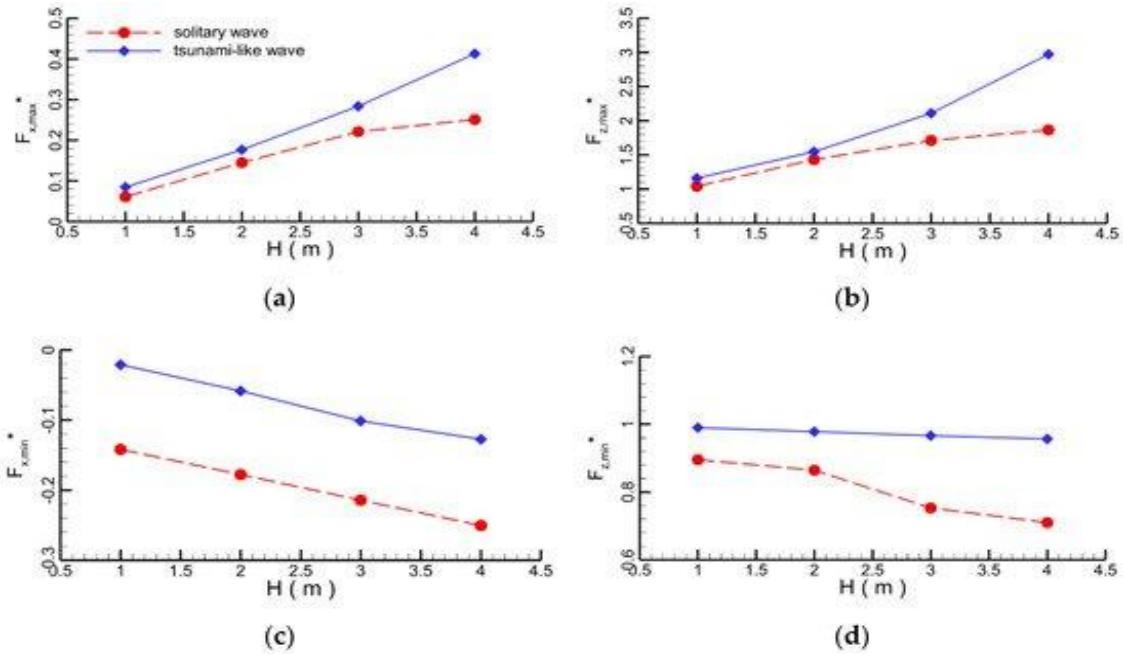

Figure 22. Plots of maximum hydrodynamic forces at the pipeline as a function of wave height; (**a**) maximum horizontal force $F_{x,max}$*; (**b**) maximum vertical force $F_{z,max}$*; (**c**) minimum horizontal force $F_{x,min}$*; (**d**) minimum vertical force $F_{z,min}$*.

4.1.3. Effect of Pipe Diameter

In ocean engineering, there are submarine pipelines with different diameters. The effects of pipeline diameter on the hydrodynamic forces of tsunami-like waves are analyzed in this section. In the computation, the water depth *h* is 10 m, wave height *H* is 2 m, and *G* = 0. Four different pipeline diameters are selected: 0.8 m, 1 m, 1.2 m, and 1.4 m. When the crest of tsunami-like wave is above the pipeline, the velocity contour of flow field around pipeline is shown in **Figure 23**. The larger the pipeline diameter, the more serious the impact of the pipeline on the surrounding flow. Under the same tsunami-like wave, the vortex behind the pipeline increases with the increase of the pipe diameter, and the high velocity region around pipeline increases too.

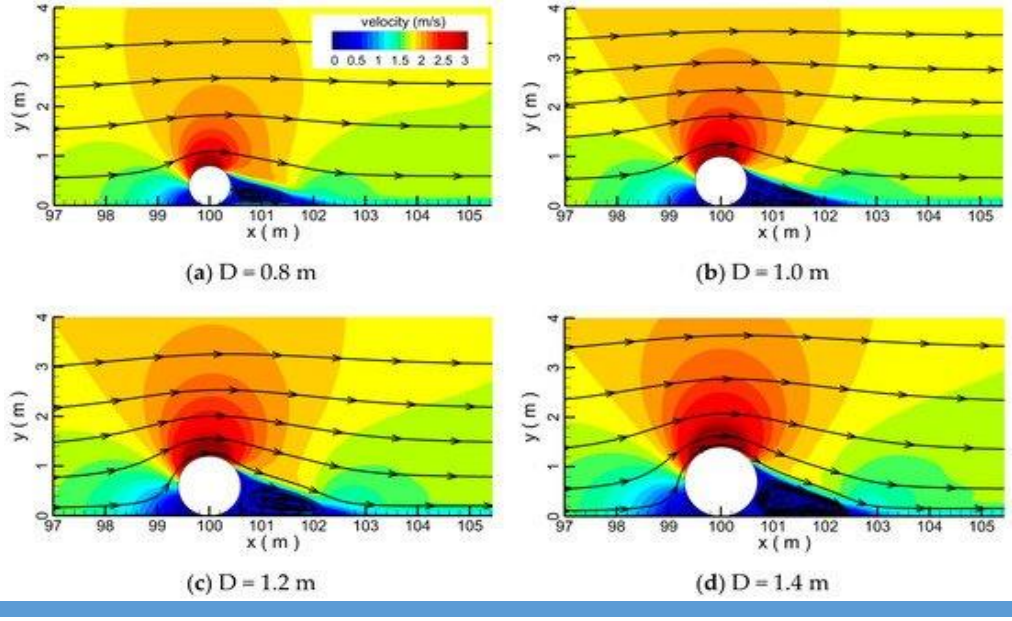

Figure 23. The velocity contours of flow fields around different size pipelines.

The maximum horizontal and vertical force functions of pipeline diameter are evaluated for the tsunami-like and solitary wave cases (**Figure 24**). In the figure, β is the ratio of pipeline diameter to the water depth. The maximums of the horizontal and vertical forces increase continuously with pipeline diameter. Meanwhile, at the same wave height, the maximum forces at the pipeline under the tsunami-like wave are always larger than under the solitary wave. It is also observed that the magnitude of the minimum of horizontal force increases as pipeline diameter increases, **Figure 24**c. However, the magnitude of the minimum vertical force decreases as pipeline diameter increases, **Figure 24**d.

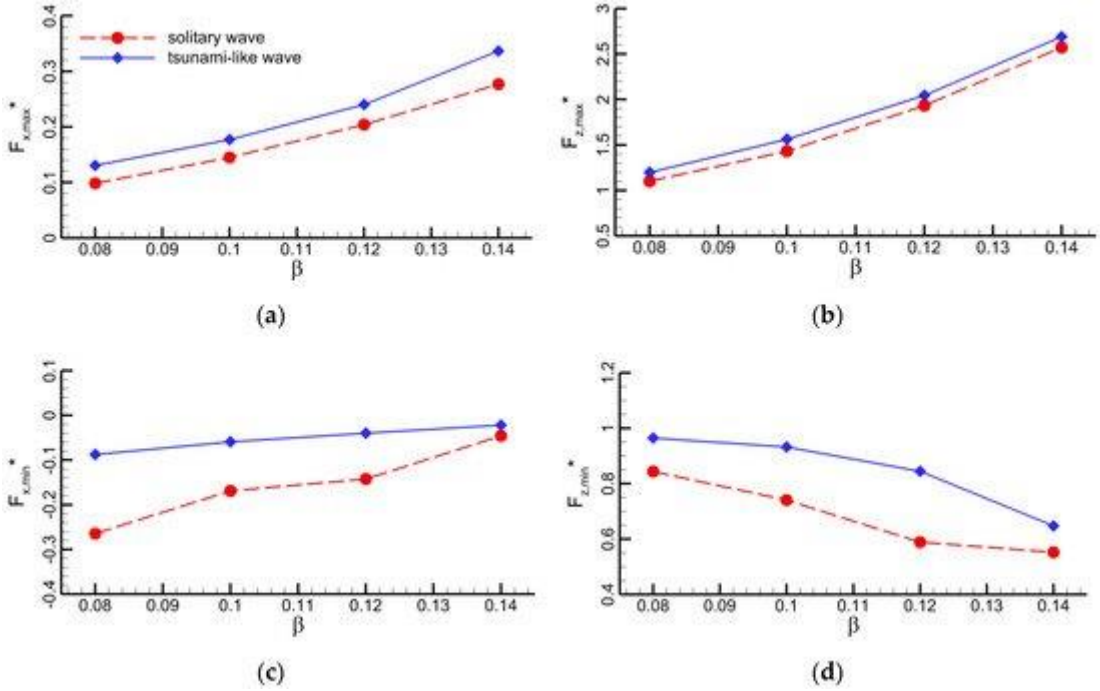

Figure 24. Plots of the maximum horizontal and vertical forces as function of pipeline diameter; (**a**) maximum horizontal force $F_{x,max}$*; (**b**) maximum vertical force $F_{z,max}$*; (**c**) minimum horizontal force $F_{x,min}$*; (**d**) minimum vertical force $F_{z,min}$*.

4.1.4. Effect of Gap-Ratio

Due to the irregular bathymetry distribution of the seabed, the submarine pipeline can have different clearance heights from the seabed. In this section, the hydrodynamic forces acting on the suspended pipelines under the tsunami-like wave are numerically analyzed with water depth h = 10 m, and wave height H = 2 m. The ratio (χ = G/D) of the gap between the pipeline and seabed to the pipeline diameter is set as 0.25, 0.5, 0.75, and 1, respectively. **Figure 25** plots the snapshots of vortices contour for pipelines with different gap-ratios at t = 135 s under a tsunami-like wave. When the pipeline is close to the seabed, the shedding vortices from the pipeline can have a strong interaction with the seabed boundary layer (**Figure 25**a). As the gap-ratio increases, the intensity of this kind of interaction gradually decreases, and detached vortices are observed, **Figure 25**b–d.

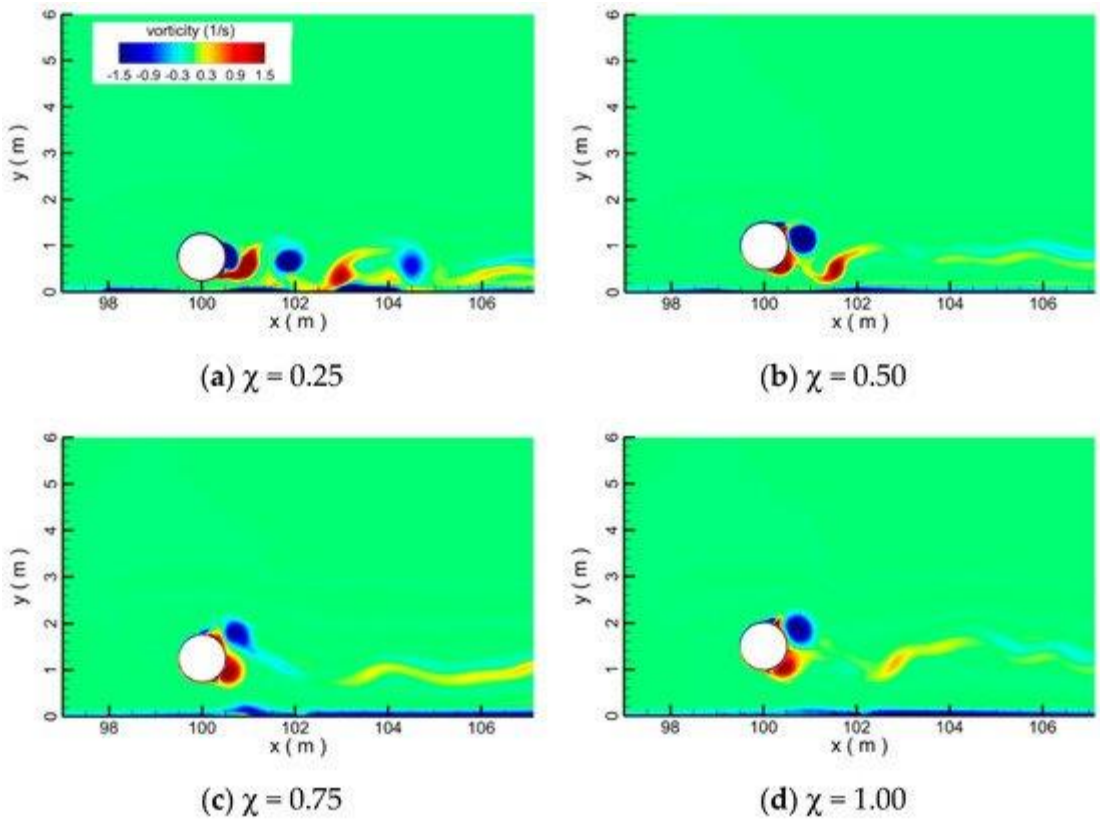

Figure 25. Snapshots of vortices contours for pipelines with different gap-ratios at t = 135 s under the tsunami-like wave.

The temporal evolution of hydrodynamic forces at the pipeline when the gap-ratio equals 0.25 is shown in **Figure 26**. It can be seen that the magnitudes of the horizontal and vertical forces are larger for the tsunami-like wave. The tsunami-like wave also has a much longer duration.

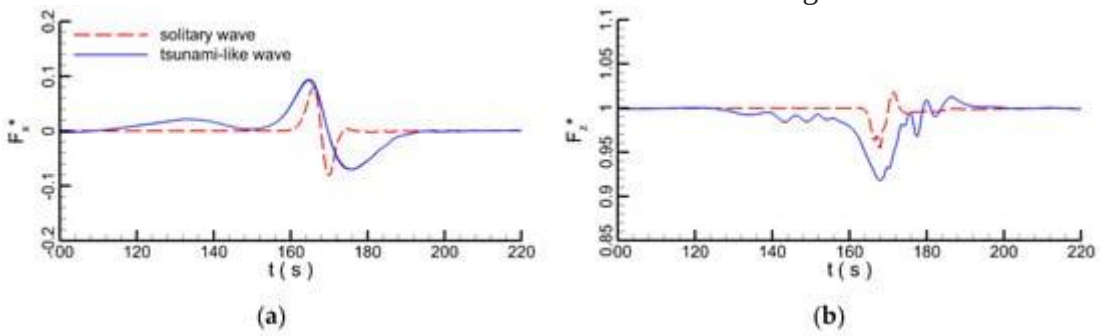

Figure 26. Temporal evolution of hydrodynamic forces at a pipeline when the gap-ratio equals 0.25; (**a**) horizontal force F_x* (**b**) vertical force F_z*.

The maxima and minima of the horizontal and vertical forces at pipeline as function of gap-ratio are plotted in **Figure 27**. As the gap ratio increases, the maximum horizontal force gradually decreases, but the rate decreases at same time. This is due to the fact that an increasing gap-ratio will substantially reduce the pressure gradient between the frontal and rear side of the pipeline, resulting in a smaller maximum horizontal force. At the same gap ratio, the maximum horizontal force for the tsunami-like wave is greater than that of solitary wave. Even if the increase of gap-ratio can reduce the pressure

gradient, the velocity of the tsunami-like wave is larger than that of a solitary wave. The larger the velocity, the larger the pressure on the pipeline. So, the pressure on the pipeline under the solitary is lower than that under the tsunami-like wave. As the gap ratio increases, the maximum vertical force decreases at a much higher rate than the maximum horizontal force. In contrast to the maximum horizontal force, the maximum vertical force for the solitary wave is greater than that of tsunami-like wave for the same gap ratio. The magnitudes of the minimum horizontal and vertical forces gradually decrease with decreasing gap-ratio (**Figure 27**c,d). The water reflux causes the minimum forces on the submarine pipeline. However, due to the gap exists below the pipeline, much more reflux water can flow through the gap, which reduces the pressure gradient around the submarine pipeline. The reflux velocity above the submarine pipeline under the tsunami-like wave is larger than that under the solitary wave. Depending on the Bernoulli equation theory, the larger the velocity above the submarine pipeline, the lower the pressure above the pipeline. So, the maximum forces under the tsunami-like wave are larger than that under a solitary wave, as shown in **Figure 27**d.

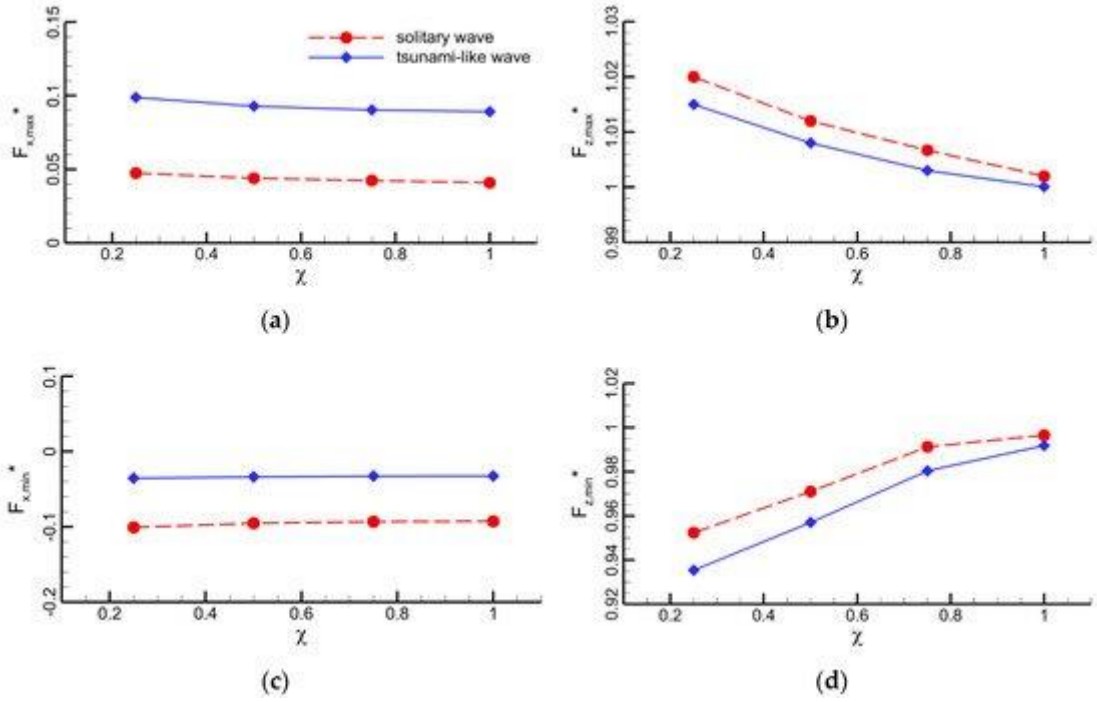

Figure 27. Plots of the maximum horizontal and vertical forces as a function of gap-ratio; (**a**) maximum horizontal force $F_{x,max}$*; (**b**) maximum vertical force $F_{z,max}$*; (**c**) minimum horizontal force $F_{x,min}$*; (**d**) minimum vertical force $F_{z,min}$*.

4.2. Pipelines in Tandem Arrangement

In this section, hydrodynamic characteristics of pipelines in tandem arrangement subjected to a tsunami-like wave are numerically investigated. The corresponding water depth *h* and wave height *H* in the computation are 10 m and 2 m, respectively. Six different spacing distances are selected: 0.5D, 1D, 1.5D, 2D, 2.5D, and 3D, respectively. The diameter *D* of the pipelines is 1 m, and the pipelines are located at $G = D$ above the seabed.

Figure 28 shows the snapshots of the vortices around the pipelines with different spacing distances for the tsunami-like wave. At 180 s, the vortices behind the single pipeline shed weakly (**Figure 28**a). When the spacing distance is 0.5 D, the shed vortices from the upstream cylinder directly interact with the boundary layer of downstream cylinder, generating a vortex street with a wide displacement in the vertical direction (**Figure 28**b). When the spacing distance is D, the intensity of

the interaction between pipelines decreases, and a series of shedding vortices in a regular pattern is observed, **Figure 28**c. If the spacing distance between pipelines is further increased, it is found that vortices shedding processes are suppressed for both upstream and downstream pipelines due to their mutual interaction, **Figure 28**d,e. When the spacing distance is 3 D, the vortices shedding process nearly disappears, **Figure 28**f. The results shown above show that the spacing distances between pipelines have significant influences on their own hydrodynamic characteristics under the impact of a tsunami-like wave.

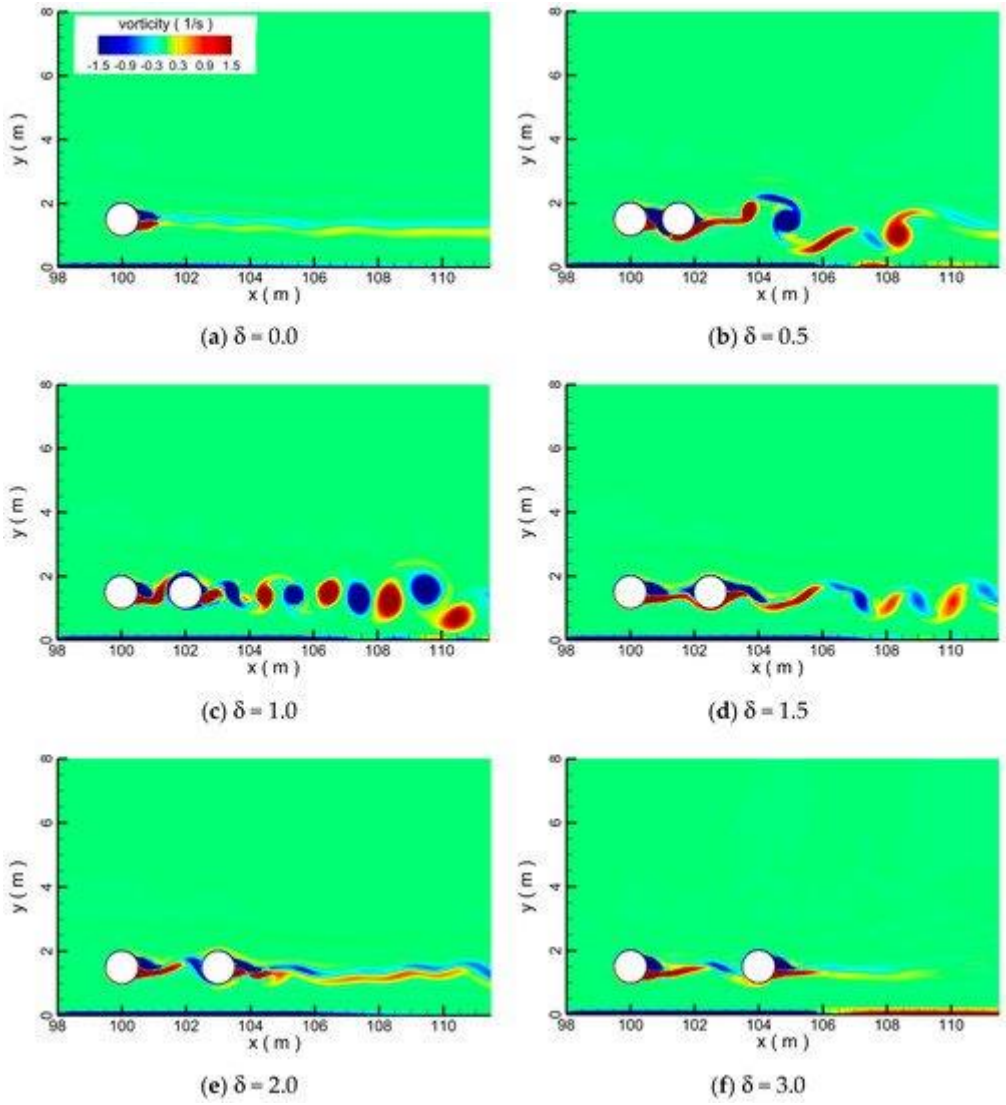

Figure 28. Snapshots of vortices contours around a tandem pipeline subjected to a tsunami-like wave at different pipeline spacing distances and t = 180 s. δ is the ratio of the distance between the two pipes to the pipeline diameter.

Compared with a tsunami-like wave (**Figure 28**), the intensity of vortices shedding processes under the solitary wave is much weaker (**Figure 29**). When the spacing distance between pipelines is 0.5 D, vortices are disturbed and in disarray (**Figure 29**b). When the spacing distance between pipelines is larger than 1 D, the influence of upstream vortices on downstream vortices is rather weak (**Figure 29**c–f).

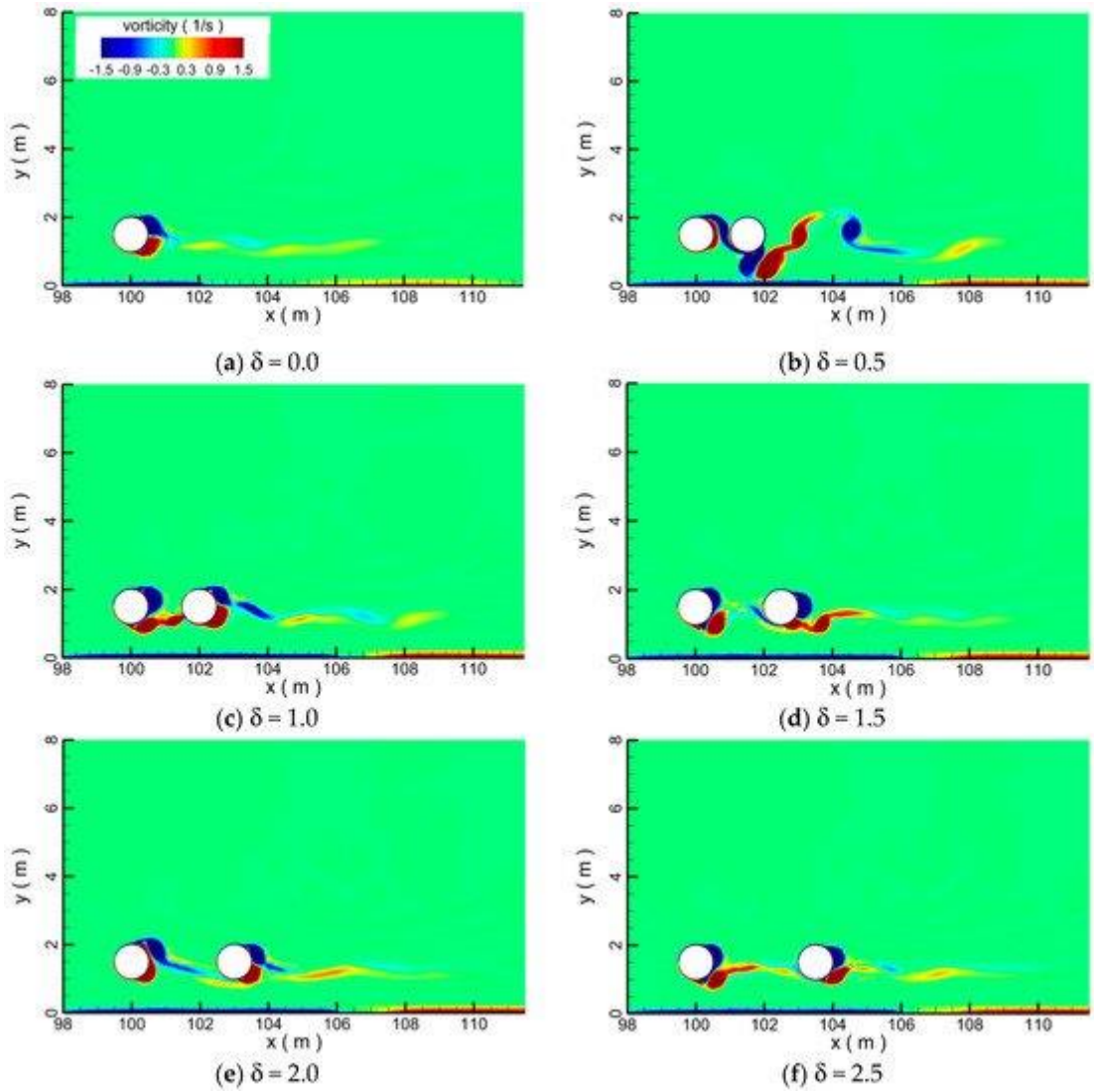

Figure 29. Same as **Figure 28** but for a solitary wave at t = 22 s.

The temporal evolutions of the hydrodynamic forces for the tandem pipeline spaced at distance 1 D are plotted in **Figure 30** for the solitary and tsunami-like wave cases. Comparing **Figure 30**a with c, the maximum horizontal peak force is greater for the downstream pipeline for both wave types. The magnitude of the horizontal forces is greater for the tsunami-like wave. The vertical forces of pipelines under the tsunami-like wave exhibit a larger oscillating pattern (**Figure 30**b,d). The vertical force amplitude is also much greater for the tsunami-like wave.

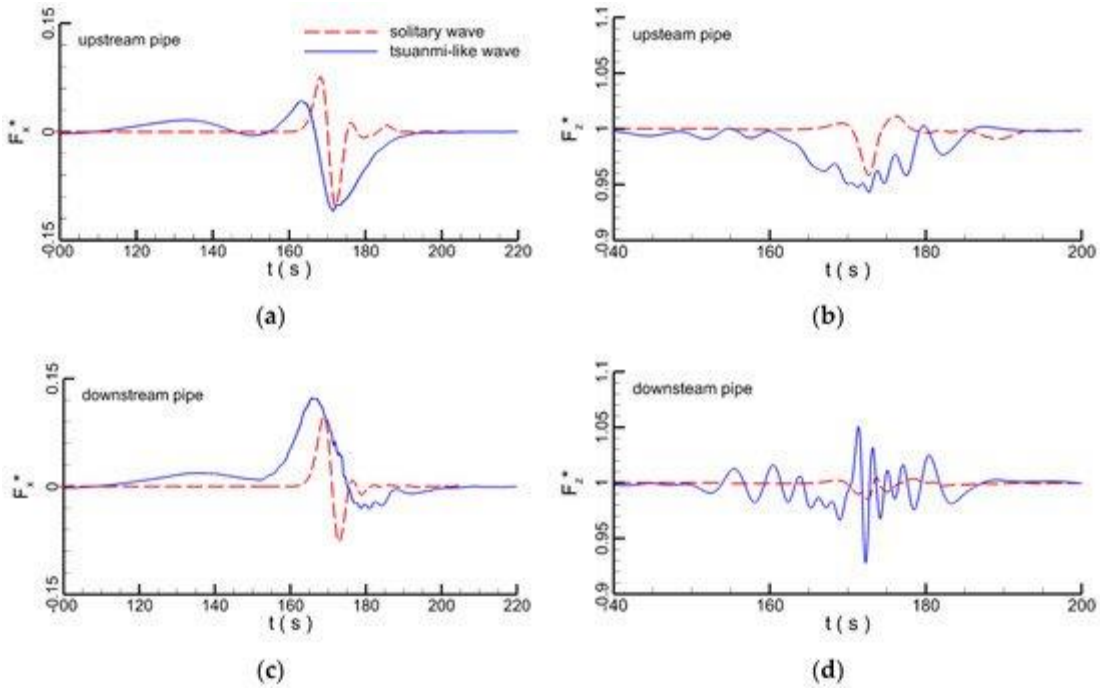

Figure 30. Temporal evolution of the hydrodynamic forces at pipelines with spacing distance 1 D under the impact of solitary and tsunami-like waves; (**a**) horizontal force of upstream pipe F_x*; (**b**) vertical force of downstream pipe F_z*; (**c**) horizontal force of downstream pipe F_x*; (**d**) vertical force of downstream pipe F_z*.

Figure 31 and **Figure 32** depict the maximum and minimum horizontal and vertical forces as a function of the spacing ratio for the pipelines. The maximum horizontal force of the upstream pipeline increases as the spacing distance increases (**Figure 31**a and **Figure 32**a). Nonetheless, the maximum horizontal force of downstream pipeline decreases. The horizontal force becomes nearly constant beyond a spacing distance greater than 2 D (**Figure 31**a,c and **Figure 32**a,c). The solitary wave also produces a greater maximum horizontal force for the upstream pipeline and a smaller maximum horizontal force for downstream pipeline, compared to the tsunami-like wave. The maximum vertical force on the upstream pipeline decreases almost linearly with the increase of spacing distance (**Figure 31**b). The tsunami-like wave produces a greater maximum vertical force for both pipelines than the solitary wave (**Figure 31**b and **Figure 32**b).

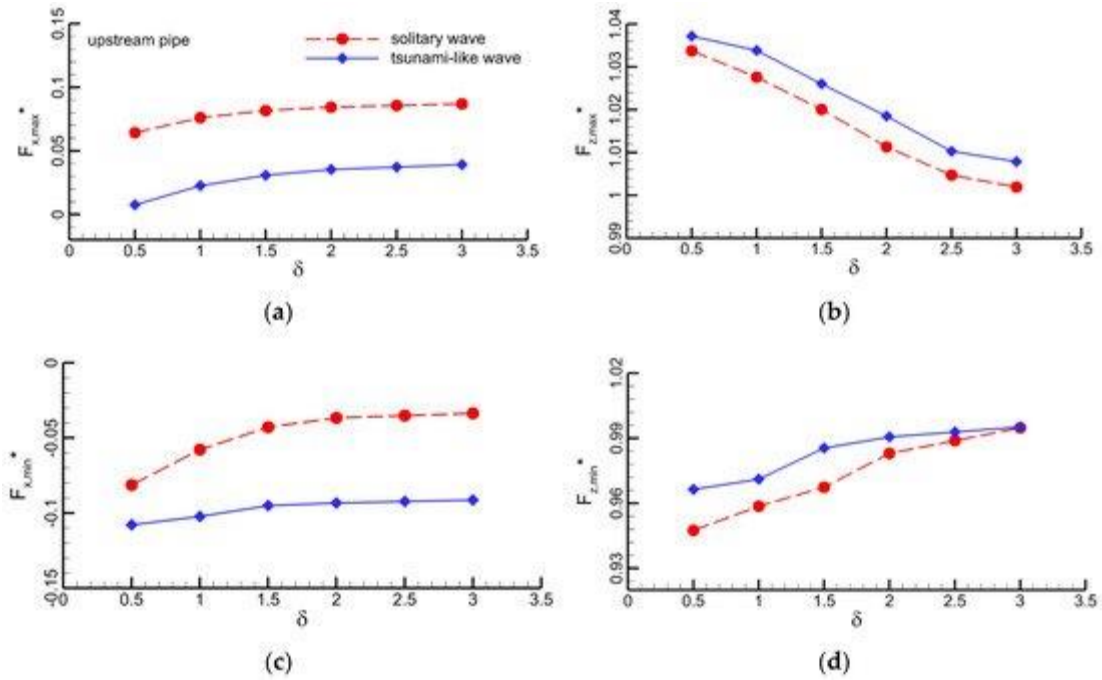

Figure 31. Horizontal and vertical forces on the upstream pipeline as function of spacing ratio; (**a**) maximum horizontal force $F_{x,max}$*; (**b**) maximum vertical force $F_{z,max}$*; (**c**) minimum horizontal force $F_{x,min}$*; (**d**) minimum vertical force $F_{z,min}$*.

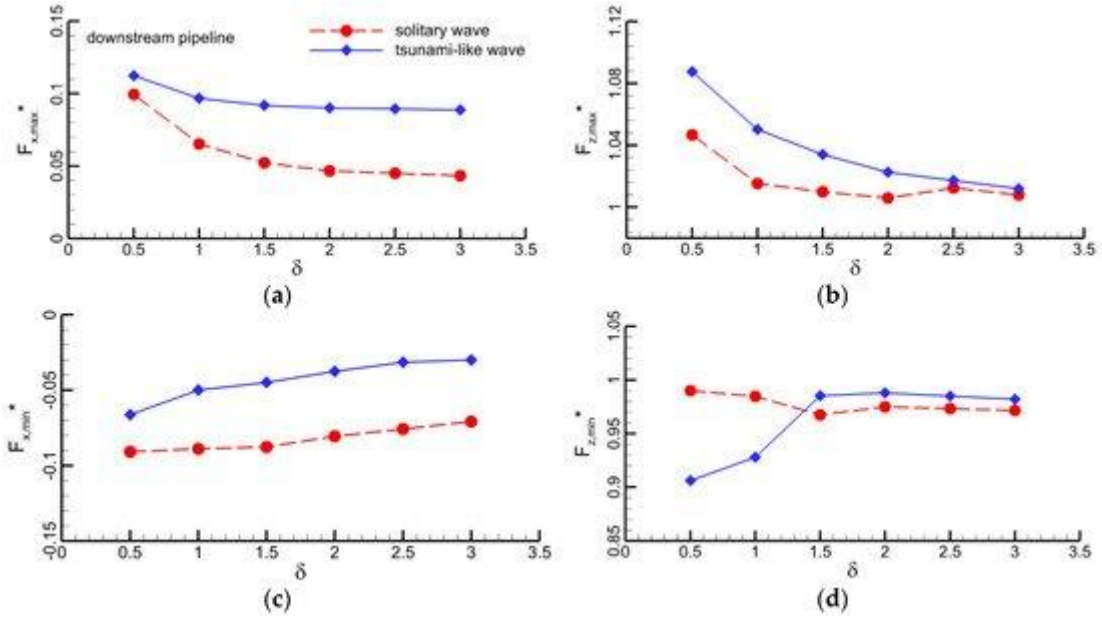

Figure 32. Horizontal and vertical forces on the downstream pipeline as function of spacing ratio; (**a**) maximum horizontal force $F_{x,max}$*; (**b**) maximum vertical force $F_{z,max}$*; (**c**) minimum horizontal force $F_{x,min}$*; (**d**) minimum vertical force $F_{z,min}$*.

5. Conclusions

This paper numerically investigates the hydrodynamic characteristics of submarine pipelines impacted by (a) a solitary wave and (b) a more realistic tsunami wave based on N-wave theory. The results strongly depend on which wave model is used. The hydrodynamic characteristics of the tsunami-like wave are drastically different from that of the solitary wave with respect to the structure of flows, force time series, water elevation, and velocity. After the tsunami-like wave has passed the pipeline, the size of the vortices at the frontal and rear sides of pipeline increases substantially. The water free surface under the tsunami-like wave is gentler than under the solitary wave, because the period of the tsunami-like wave is longer than that of the solitary wave. After the solitary wave has passed the pipeline, the vortices behind the pipeline are much smaller than for the tsunami-like wave. When they pass through the pipeline, wave heights decrease for both waves. The wave height of the solitary wave decreases by more than that of the tsunami-like wave. For the tsunami-like wave, the vortex behind the pipeline increases with the increase of pipe diameter. It is also found that hydrodynamic forces at submarine pipelines also may strongly depend on wave height, water depth, pipeline diameter, and gap-ratio. Maximum forces increased with wave height and pipeline diameter. However, the maximum horizontal force decreases with increasing water depth and distance between pipeline and seabed. For the same wave height, the duration of the acting force is much longer for the tsunami-like wave. Overall, the hydrodynamic forces experienced by submarine pipelines are relatively greater when the tsunami-like wave model is used.

The hydrodynamic forces acting on pipelines in tandem arrangement were also discussed. The spacing distance between upstream and downstream pipelines has a significant influence on the forces of the tandem pipeline and the flow field. When the spacing distance is 0.5 D, the shed vortices from the upstream cylinder directly interact with the boundary layer of the downstream cylinder, generating a vortex with wide displacement in the vertical direction. When the spacing distance is D, the intensity of the interaction between the pipelines decreases significantly, and a series of shedding vortices in a regular pattern is observed. With increasing spacing distance, the maximum horizontal (vertical) forces decreased (increased) continuously at both pipelines. The horizontal forces became nearly constant when the spacing distance exceeds 2 D. All of the discussion presented above supports the idea that modelling real tsunami waves using the solitary wave model is relatively inaccurate, and that improved wave models should be used instead.

In offshore oil fields, the submarine pipelines are laid on seabed with varying topography. In submarine pipeline construction, whether the seabed is smooth (i.e., relatively flat) or uneven (corrugated, with high points and low points) should be considered as the primary physical factor. If the bed is uneven, the pipeline may include free spans with unsupported sections. If an unsupported section is too long, the bending stress exerted onto it (due to its weight or marine factors) may be excessive. Vibrations from current-induced vortices may also induce the destruction of submarine pipelines. Since most submarine pipelines are laid on flat seabed, in this study, flat seabed was considered. If slopes exist on the seabed, the numerical results will be affected to some extent. Once the waves run up along the slope, the characteristics of the wave change significantly and the broken flow causes different effects on the submarine pipeline. In future research, we will study the effect of tsunami-like waves on submarine pipelines laid on sloped seabed.

Author Contributions

Conceptualization, E.Z. and K.Q.; Methodology, E.Z. and K.Q.; Validation, E.Z. and K.Q.; Formal Analysis, L.M.; Investigation, E.Z.; Resources, E.Z. and K.Q.; Writing-Original Draft Preparation, E.Z.; Writing-Review & Editing, L.M., K.Q., S.K. and B.S.; Supervision, L.M.; Funding Acquisition, L.M.

Funding

This research was funded by the National Key Research and Development Program of China (Grant No. 2017YFC1404700), the National Natural Science Foundation of China (Grant No. 51809021, and 51839002), the Discipline Layout Project for Basic Research of Shenzhen Science and Technology Innovation Committee (Grant No. 20170418), the Guangdong Special Fund Program for Marine Economy Development (Grant No. GDME-2018E001), and the Fundamental Research Funds for the Central Universities, China University of Geosciences (Wuhan) (Grant No. 2018379010).

References

Fang, N.; Chen, G.M.; Zhu, H.W.; Meng, H.X. Statistical analysis of leakage accidents of submarine pipeline. Oil Gas Storage Transp. 2014, 33, 99–103. [Google Scholar]

Tong, F.F.; Cheng, L.; An, H.; Griffiths, T. The hydrodynamic forces on a circular cylinder in proximity to a wall with intermittent contact in steady current. Ocean Eng. 2017, 146, 424–433. [Google Scholar] [CrossRef]

Sumer, B.M.; Fredsoe, J.; Gravesen, H.; Bruschi, R. Response of Marine Pipelines in Scour Trenches. J. Waterway Port Coast. Ocean Eng. 1989, 115, 477–496. [Google Scholar] [CrossRef]

Zhao, E.J.; Shi, B.; Qu, K.; Dong, W.B.; Zhang, J. Experimental and Numerical Investigation of Local Scour around Submarine Piggyback Pipeline under Steady Currents. J. Ocean Univ. China 2018, 17, 244–256. [Google Scholar] [CrossRef]

Subbiah, K.; Cheong, H.F.; Shankar, N.J. Regular and random wave pressures around large diameter submarine pipeline near ocean bed. J. Hydraul. Res. 1991, 29, 49–66. [Google Scholar] [CrossRef]

Gao, F.P.; Gu, X.Y.; Jeng, D.S.; Teo, H.T. An experimental study for wave-induced instability of pipelines: The breakout of pipelines. Appl. Ocean Res. 2002, 24, 83–90. [Google Scholar] [CrossRef]

Haley, J.F.; Swan, C.; Gibson, R. An Experimental Investigation of Wave Impact Loads on a Slender Horizontal Cylinder. In Proceedings of the ASME 2014 33rd International Conference on Ocean, Offshore and Arctic Engineering, San Francisco, CA, USA, 8–13 June 2014; American Society of Mechanical Engineers: New York, NY, USA, 2014; p. V08BT06A041. [Google Scholar]

Gao, N.; Yang, J.; Li, X.; Zhao, W. Wave forces on horizontal cylinder due to nonlinear focused wave groups. In Proceedings of the Twenty-fifth International Ocean and Polar Engineering Conference, Kona, HI, USA, 21–26 June 2015; International Society of Offshore and Polar Engineers: Houston, TX, USA, 2015. [Google Scholar]

Chern, M.-J.; Odhiambo, E.A.; Horng, T.-L.; Borthwick, A.G.L. Numerical simulation of vibration of horizontal cylinder induced by progressive waves. Fluid Dyn. Res. 2016, 48, 015508. [Google Scholar] [CrossRef][Green Version]

Ong, M.C.; Kamath, A.; Bihs, H.; Afzal, M.S. Numerical simulation of free-surface waves past two semi-submerged horizontal circular cylinders in tandem. Mar. Struct. 2017, 52, 1–14. [Google Scholar] [CrossRef]

Liang, D.F.; Gotoh, H.; Khayyer, A.; Chen, J.M. Boussinesq mdelling of solitary wave and N-wave runup on coast. Appl. Ocean Res. 2013, 42, 144–154. [Google Scholar] [CrossRef]

Hsiao, S.C.; Lin, T.C. Tsunami-like solitary waves impinging and overtopping an impermeable seawall: Experiment and RANS modeling. Coast. Eng. 2010, 57, 1–18. [Google Scholar] [CrossRef]

Limura, K.; Norio, T. Numerical simulation estimating effects of tree density distribution in coastal forest on tsunami mitigation. Ocean Eng. 2012, 54, 223–232. [Google Scholar]

Synolakis, C.E. The run-up of solitary waves. J. Fluid Mech. 1987, 185, 523–545. [Google Scholar] [CrossRef]

Gedik, N.; Irtem, E.; Kabdasli, S. Laboratory investigation on tsunami run-up. Ocean Eng. 2005, 32, 513–528. [Google Scholar] [CrossRef]

Goseberg, N.; Wurpts, A.; Schlurmann, T. Laboratory-scale generation of tsunami and long waves. Coast. Eng. 2013, 79, 57–74. [Google Scholar] [CrossRef]

Francesco, A.; Tripepi, G.; Meringolo, D.D.; Veltri, P. Solitary wave-induced forces on horizontal circular cylinders: Laboratory experiments and SPH simulations. Coast. Eng. 2017, 129, 17–35. [Google Scholar]

Madsen, A.; Schäffer, H.A. Analytical solutions for tsunami run-up on a plane beach: Single waves, N-waves and transient waves. J. Fluid Mech. 2010, 645, 27–57. [Google Scholar] [CrossRef]

Madsen, A.; Fuhrman, D.R.; Schäffer, H.A. On the solitary wave paradigm for tsunamis. J. Geophys. Res. 2008, 113, 286–292. [Google Scholar] [CrossRef]

Chan, I.C.; Liu, L.F. On the run-up of long waves on a plane beach. J. Geophys. Res. 2012, 117, 72–82. [Google Scholar] [CrossRef]
Qu, K.; Ren, X.Y.; Kraatz, S. Numerical investigation of tsunami-like wave hydrodynamic characteristics and its comparison with solitary wave. Appl. Ocean Res. 2017, 63, 36–48. [Google Scholar] [CrossRef]
Stefan, L.; Oumeraci, H. Solitary waves and bores passing three cylinders-effect of distance and arrangement. Coast. Eng. Proc. 2014, 1, 39. [Google Scholar]

Istrati, D.; Buckle, I.; Lomonaco, P.; Yim, S. Deciphering the Tsunami Wave Impact and Associated Connection Forces in Open-Girder Coastal Bridges. J. Mar. Sci. Eng. 2018, 6, 148. [Google Scholar] [CrossRef]

Zhao, E.J.; Mu, L.; Shi, B. Numerical Study of the Influence of Tidal Current on Submarine Pipeline Based on the SIFOM–FVCOM Coupling Model. Water 2018, 10, 1814. [Google Scholar] [CrossRef]

Rhie, T.M.; Chow, A. Numerical study of the turbulent flow past an isolated airfoil with trailing-edge separation. AIAA J. 1983, 21, 1525–1532. [Google Scholar] [CrossRef]

Gomes, M.N.; Olintoa, C.R.; Rochaa, L.A.O.; Souzaa, J.A.; Isoldi, L.A. Computational modeling of a regular wave tank. Therm. Eng. 2009, 8, 44–50. [Google Scholar]

Hafsia, Z.; Haj, M.B.; Lamloumi, H.; Maalel, K. Comparison between Moving Paddle and Mass Source Methods for Solitary Wave Generation and Propagation over A Steep Sloping Beach. Eng. Appl. Comput. Fluid Mech. 2009, 3, 355–368. [Google Scholar] [CrossRef]

Qu, K.; Ren, X.Y.; Kraatz, S.; Zhao, E.J. Numerical analysis of tsunami-like wave impact on horizontal cylinders. Ocean Eng. 2017, 145, 316–333. [Google Scholar] [CrossRef]

Sibley, P.O. The Solitary Wave and the Forces It Imposes on a Submerged Horizontal Circular Cylinder: An Analytical and Experimental Study. Ph.D. Thesis, City University London, London, UK, 1991. [Google Scholar]

References

Zhao, E., Qu, K., Mu, L., Kraatz, S., & Shi, B. (2019, January 29). Water | Free Full-Text | Numerical Study on the Hydrodynamic Characteristics of Submarine Pipelines under the Impact of Real-World Tsunami-Like Waves | HTML. MDPI; www.mdpi.com. https://www.mdpi.com/2073-4441/11/2/221/htm

Schrecker, A. M. (1978, September 0). The University of Cape Town . Wave Forces on Submarine Piplines. https://open.uct.ac.za/bitstream/item/20729/thesis_ebe_1978_schrecker_arnold_malan.pdf?sequence=1